Structural foundations of resting-state and task-based functional connectivity in the human brain

A. M. Hermundstad[1], D. S. Bassett[1,2], K. S. Brown[1,3,4], E. M. Aminoff[5], D. Clewett[6], S. Freeman[7], A. Frithsen[8], A. Johnson[8], C. Tipper[8], M. B. Miller[8], S. T. Grafton[8] and J. M. Carlson[1]

[1]Department of Physics, University of California, Santa Barbara, CA USA
[2]Sage Center for the Study of the Mind, University of California, Santa Barbara, CA USA
[3]Department of Chemical, Materials, and Biomolecular Engineering, University of Connecticut, Storrs, CT USA
[4]Department of Marine Sciences, University of Connecticut, Groton, CT USA
[5]Center for the Neural Basis of Cognition, Carnegie Mellon University, Pittsburgh, PA USA
[6]Neuroscience Graduate Program, University of Southern California, Los Angeles, CA USA
[7]Department of Psychology, University of California, San Diego, CA USA
[8]Department of Psychological and Brain Sciences, University of California, Santa Barbara, CA USA

February 14, 2013

Supporting Information

CONTENTS

SUMMARY

The following Supporting Information details specific methodology and supplemental results that support the findings of the main text. In Supplemental Methods, we discuss the experimental and computational acquisition of structural and functional connectivity measures related in the main text. In Supplemental Results, we confirm that the observed relationships between structural and functional connectivity are robust to variations in our analysis techniques.

Supplemental Methods. In the main text, we assessed structural and functional connectivity between 600 brain regions across 84 subjects. Structural connectivity was defined by the number and length of white matter tracts linking brain regions, and functional connectivity was defined by the strength of BOLD correlations between brain regions measured at rest, during the performance of an attention task, and during the performance of a facial recognition memory task. Here, we discuss the experimental and computational procedures used to acquire these measurements. We first provide details about the subjects that participated in this study. We then describe the experimental conditions, including the specifications of an additional word recognition memory task, under which the structural and functional data was collected. Finally, we discuss the estimation of structural and functional connectivity from this data.

Supplemental Results. In the main text, we used structural and nonstructural measures to identify pairs of brain regions that were consistently structurally connected within a large percentage of subjects. Within the subset of regions selected via these measures, we constructed subject-averaged ("representative") and subject-specific brain networks from measures of structural and functional connectivity. We examined the extent to which functional connectivity could be inferred from structural connectivity, and to what extent structural connectivity could be inferred from functional connectivity. Subgroups of connections partitioned based on structural and functional measures (lower left and upper right of Figure 1 in the main text) were shown to differ in their strength of functional and structural connectivity (Figures 2 and 3 in the main text). Here, we highlight the specific anatomical regions of the brain involved in these structural and functional connections. We then show that the observed relationships between structural and functional connectivity are robust to the specific choices made in selecting and partitioning subgroups of connections. By comparing two memory tasks, one for faces (assessed in the main text) and one for words (assessed in this supplement), we confirm that the observed properties of memory-state functional connectivity are consistent across different memory conditions. Finally, we discuss the sensitivity of these results to inconsistent structural connectivity within representative and subject-specific brain networks.

We conclude by highlighting additional methodological considerations and their potential implications on the work presented here.

MATERIALS AND METHODS

Study Subjects

133 people were designated to participate in this study. 38 of the subjects were not used in the final analysis due to the following reasons: 8 subjects did not pass MRI safety screening measures; 4 subjects were claustrophobic; 5 subjects had a technical error in data collection; 20 subjects missed more than 40 trials (over 10% of the trials) in either the memory for words or memory for faces test; 1 subject did not follow task instructions.

Of the remaining 95 subjects, 11 had missing or unusable diffusion imaging data. We therefore analyzed data from 84 subjects: ages 27-45 (mean 34.21, standard deviation 4.23); 4 females, 80 males; 12 left-handed. None of the subjects were color blind. Informed written consent was obtained from each subject prior to the experimental sessions. All procedures were approved by the University of California, Santa Barbara Human Subjects Committee.

Experimental Tasks

Structural and functional brain scans were performed at the UCSB Brain Imaging Center. Functional scans were acquired during four different experimental states: resting, attention, memory for faces, and memory for words [1].

MRI Data Acquisition

Functional and structural scans were acquired using a research-dedicated, phased array 3T Siemens TIM Trio with a standard 12 channel head coil. Cushions were placed around the head to minimize head motion. Subjects held in their right hand an MRI compatible, two-button response box and in their left hand a squeeze ball for emergency

purposes. Experimental stimuli were projected on a screen behind the supine subject, and a mirror mounted on the head coil reflected the images from the screen into the subject's field of view.

Functional Scans. Functional runs consisted of a T2*-weighted single shot gradient echo, echo-planar sequence sensitive to BOLD contrast (TR = 2.5s, TE = 30ms, FA = 90°) with generalized autocalibrating partially parallel acquisitions (GRAPPA; 64×64 matrix, 192mm×192mm FOV). Each volume consisted of 37 slices acquired parallel to the AC-PC plane, although the angle was slightly adjusted to optimize for frontal acquisition if necessary (interleaved, 3mm thickness with .5mm gap; 3mm×3mm in-plane resolution). Each functional scanning run began with the acquisition of four dummy volumes used to achieve steady-state tissue magnetization, which were later discarded. A transistor-transistor logic (TTL) pulse sent out by the scanner at the onset of each viable EPI volume triggered the stimulus presentation software, and synched the beginning of each trial to the onset of the next complete image volume.

Once each subject was positioned in the scanner, anatomical and memory task functional scans were acquired first, followed by three blocks of attention task trials. A total of 146 volumes was acquired during the resting-state scan, for which subjects were instructed to remain still, keep their eyes open, and look at the blank screen. Note that these resting-state scans are similar in length to those used in previous studies to identify meaningful resting state networks [2, 3, 4, 5], and they are significantly longer than those used to examine the temporal evolution of brain network dynamics [2, 6]. A total of 540 volumes was acquired for each of the two memory test runs (faces and words), each consisting of 360 stimulus trials and 180 fixation trials. A total of 240 volumes was acquired for each of two attention task runs. The details of the experimental setup, stimuli, and testing conditions for the memory and attention tasks are described in the subsequent sections.

Structural Scans. Structural scans were acquired between memory test runs (see 'Memory Tasks; Overall Procedure') using an echo planar diffusion weighted technique acquired with iPAT and an acceleration factor of 2. The timing parameters of the pulse sequence were TE/TR = 94/8400ms, 30 diffusion directions with a maximal b-value of 1000s/mm^2 and two averages. Two $b0$ images were acquired during the DTI scan. The matrix size was 128×128 and the slice number was 60. The field of view was 230×230mm^2 and the slice thickness 2mm. The acquisition time per DTI scan was 9:08min.

In addition to the diffusion scan, a three dimensional (3D) high-resolution T1-weighted sagittal sequence image of the whole brain was obtained by a magnetization prepared rapid acquisition gradient-echo (MPRAGE) sequence with the following parameters: TR = 2300; TE = 2.98ms; flip angle = 9°; 160 slices; 1.10mm thickness.

Memory Tasks

360 faces and 360 words were used as stimuli in the memory task experiment. Faces of varying ethnicity were depicted in black and white photographs of size 2.78in by 3.33in. Words were four to eight letters in length. Words in the target and distracter lists were matched for imageability (range 502-655) and frequency (range 1-382; Kucera-Francis written frequency count) as evaluated through the MRC Psycholinguistic Database. Words were presented in Arial font with a font size of 40. Stimuli were counter-balanced across subjects and conditions.

Experimental Procedure. Both memory tasks consisted of a study session, during which subjects were not scanned, followed by a test session held approximately 9 minutes after the study session, during which subjects were scanned.

Overall Procedure. To familiarize subjects with the task prior to entering the scanner, each subject participated in a short practice session. The practice included separate study sessions of 15 words and 15 faces, and separate test sessions of 30 words and 30 faces, respectively. Once comfortable with the task, subjects were placed in the MRI scanner and underwent a localizer scan that lasted a few seconds. Subjects were reminded of instructions before beginning the first study session, consisting of either faces or words, during which imaging data was not collected. Once completed, an anatomical scan was acquired over nine minutes, during which a screen saver was presented on the screen. Subjects were then reminded of the instructions for the test session, and functional MRI scans were collected while subjects performed the recognition memory test on the set of either face- or word-stimuli (depending on the preceding study session). Immediately following the first study-test session, subjects participated in the second study-test session. The first and second study-test sessions were separated by a delay of 9 minutes during which another anatomical scan was acquired. Each subject had separate study-test sessions for each set of face- or word-stimuli in which the order (first or second study-test for words versus faces) was counter-balanced.

Study Session. 180 stimuli, consisting of either words or faces, were presented sequentially in the center of the screen against a white background. Words were presented in black font, and faces were presented without a frame. Face- and word-stimuli were shown for 1s or 1.5s, respectively. In both cases, sequential stimuli were separated by a 1s inter-trial-interval. Subjects were instructed to remember each stimulus for a later memory test. To facilitate deep encoding of the faces stimuli, which were harder to remember, subjects responded as to whether each face was pleasant or unpleasant via a button press. Words were viewed passively.

Test Session. Each test consisted of the 180 previously-studied stimuli and 180 novel stimuli. Test stimuli were divided into two conditions: a High Probability condition in which there a 70% probability that the stimulus was old (i.e., studied previously), or a Low Probability condition in which there was a 30% probability that the stimulus was old. Probability condition was cued via font color for words (red or green) or a colored, rectangular frame for faces (red or green). The association between color and condition was counter-balanced. Stimuli were presented at the same size and location as in the study session, again displayed for 1.5s with a 1s inter-trial-interval.

Subjects were instructed to determine whether the stimulus was previously studied and to press the respective button for a response of an "old" versus "new" stimulus. Instructions to the subjects included explicit information about the color cue, which indicated the probability that the stimulus was old. Subjects were informed of the color that indicated a 70% likelihood that the stimulus was old and thus highly likely to have been seen during the study session, and similarly of the color that indicated a 30% likelihood that the stimulus was old and was therefore most likely to be a novel stimulus not presented during the study session. Subjects were told that these were accurate probabilities and there were no hidden tricks. However, the instructions did not explicitly tell the subject to incorporate the probability into the memory judgment. Stimuli were presented in a pseudo-block format in which six to nine trials of the same probability were presented before the probability switched. Old and new stimuli were intermixed within these blocks. The probability indicated by the color cue did not necessarily correspond to the proportion of old and new stimuli within each mini-block of 6-9 sequential trials, but rather to the distribution of old and new stimuli within the overall test session. Intermixed throughout the entire test session were 180 fixation trials in which a black '+' symbol was displayed at the center of the screen for 2.5s.

Attention Task

Strategic Attention Task and Stimuli. The strategic attention task employed a modified spatial cueing procedure [7] in which subjects were asked to view sequences of visual stimuli, presented in blocks of discrete experimental trials, and discriminate test displays for the presence or absence of a pre-specified target stimulus. Each trial consisted of a 250ms presentation of a blank screen, followed by the sequential presentation of a fixation cross ('+'), an arrowhead cue stimulus, and a test display in which a target could be present or absent. The background color of the display screen was light gray, the arrowhead cue could be green or red, and all other stimuli were black. The fixation cross appeared at the center of the viewing screen for a randomly selected duration between 400ms and 600ms and was subsequently replaced by an arrowhead cue pointing to the left or to the right of center. The cue provided two important pieces of information that subjects could use to strategically prepare for the upcoming test display. The color of the arrowhead (either red or green) indicated the likelihood that the target would be present in the subsequent test display, such that one arrow color indicated a 70% likelihood that the target would appear, while the other color indicated 30% likelihood. The direction of the arrowhead indicated the probable (75%) location of the target should it appear at all. Within a random time interval between 1400ms and 160ms following the cue onset, a test display was presented in which two small rectangles appeared for approximately 50ms (3 vertical refreshes at 60Hz), one on each side of the cue. Horizontal rectangles were defined as targets, while vertical rectangles were defined as distractors. Each test display contained either one target stimulus and one distractor (target present condition), or two distractors (target absent condition). The test display was replaced by a central fixation cross for an inter-trial interval that varied between 1200ms and 3200ms. Immediately following each test display, subjects were required to make a two-alternative forced choice button press response as quickly and accurately as possible to indicate whether or not a target had been present.

Stimulus presentation was controlled with a Macintosh Powerbook G4 laptop computer (Apple, Inc.) running the Mac OS X 10.4 operating system, and programmed using MATLAB 7.5 (The Mathworks, Inc.) and the Psychophysics Toolbox extensions [8, 9]. Subjects performed a brief practice session prior to entering the scanner, for which subjects were seated at a desk and stimuli were presented on a 19in LCD computer monitor. Once inside the scanner, subjects were supine and viewed stimuli on a mirror reflecting display images that were back-projected onto a screen at the head of the scanner bore. The size of the stimulus display was 1024×768 pixels. The viewing mirror in the scanner was 16cm by 8cm and was positioned approximately 16cm from subjects' eyes. These dimensions produced a viewing angle that spanned approximately 53° horizontally and approximately 41° vertically. The fixation cross subtended

26×26 pixels (approximately $1.5° \times 1.5°$). The test display rectangles were presented 324 pixels (approximately $17.5° \times 17.5°$) to the left or right of the center of the screen and had minimum and maximum dimensions of 4 and 50 pixels (approximately $0.25°$ and $2.75°$).

Procedure. Prior to testing, each subject was provided with instructions regarding task executions. On each trial, each subject was informed of the probabilistic information regarding target likelihood and location provided respectively by the color and cue direction. However, subjects were not told how to apply this information to their performance of the target discrimination task. It was therefore up to each subject to decide whether and how to use cue information to strategically prepare for the test display. Following instructions, a 5min practice session was completed outside the scanner during which subjects were free to ask questions and experimenters could ensure that the task was performed correctly.

The first block of trials, during which functional scans were not performed, was used as a psychophysical calibration that normalized task difficulty across subjects by determining customized dimensions for the test display rectangles. In this calibration block, performance was assessed and the dimensions of the target rectangle were adjusted on a trial-by-trial basis using an adaptive Bayesian algorithm implemented in the QUEST psychometric routines for MATLAB and the Psychophysics toolbox [10, 11]. Based on cumulative accuracy, the QUEST algorithm suggested dimensions for test display rectangles after each trial such that task difficulty was modulated to keep overall accuracy near 70%. Test display rectangles were initially sized at 8 pixels by 31 pixels (approximately $0.5° \times 1.75°$). Difficulty was increased by making rectangles shorter and wider (closer to square, with less differentiation between horizontal and vertical) and decreased by making them longer and thinner (further from square, with more differentiation between horizontal and vertical). The dimensions determined at the end of the calibration block were then used in the subsequent two blocks of trials during which functional scans were acquired.

A total of 112 trials were presented during each experimental block. Thirty-two of these were fixation-only trials, in which subjects maintained fixation on the central cross, but neither cue nor target stimuli appeared. Of the remaining 80 trials, 40 (50%) presented a cue colored to indicate a likely target, and 40 (50%) presented a cue colored to indicate an unlikely target. Of the 40 likely target trials, 28 (70%) actually contained targets. Of these 28 target-present trials, 21 (75%) presented valid targets that appeared at the cued location, and 7 (25%) presented invalid targets that appeared opposite the cued location. Of the 40 unlikely target trials, 12 (30%) actually contained targets. Of these 12 target-present trials, 9 (75%) presented valid targets and 3 (25%) presented invalid targets. Two types of cue arrows, right- and left-pointing, were presented with equal frequency.

A rapid event-related fMRI design was employed in order to present a pseudo-random sequence of trials within each scanning run. Trial sequencing was determined uniquely for each scanning run using an m-sequence clustering algorithm, implemented in MATLAB, that maximized the power and efficiency of the experimental design by clustering repetitions of each experimental condition through five iterations in order to achieve an optimal balance between a fully randomized and a fully blocked sequence [12].

Connectivity Estimates

Functional connectivity was estimated from fMRI measurements acquired during each of the four experimental states: resting, attention, memory for words, and memory for faces. Structural connectivity was estimated from the tractographic reconstruction of white matter pathways obtained from DTI measurements.

Functional Connectivity

fMRI Data Preprocessing. Translational and rotational head movement was consistently small across subjects and datasets. The distributions of maximal translation and rotation from TR to TR were the same for rest, attention, memory for faces, and memory for word runs, with mean translational (μ_T) and rotational (μ_R) values of $\mu_T = [0.0787 \pm 0.0039\text{mm}, 0.0719 \pm 0.0043\text{mm}, 0.0513 \pm 0.0030\text{mm}, 0.0536 \pm 0.0037\text{mm}]$ and $\mu_R = [0.0493 \pm 0.0027°, 0.0503 \pm 0.0041°, 0.0362 \pm 0.0022°, 0.0391 \pm 0.0029°]$, reported here with the standard error of the mean. The largest maximum values of translation and rotation, measured across subjects and datasets, were 0.34mm and 0.33°, respectively.

Functional images were realigned to correct for these head movements by registering all images to the first image in the time series. To further correct for noise-driven demagnetization and signal loss, heavily noisy task-related images with large global residuals were given decreased weight in the generalized linear model (as implemented via the robust weighted least squares toolbox, http://www.icn.ucl.ac.uk/motor control/imaging/robustWLS.html). Functional images were then coregistered to the anatomical image. The anatomical image was normalized, using combined segmentation and normalization, to conform to the Montreal Neurological Institute (MNI)152 template. The parameters of this transformation were applied to the functional images, which were re-sampled to 2mm isotropic

voxels. Functional images were then smoothed using an isotropic Gaussian kernel (FWHM = 8mm). BOLD signals arising from any cerebrospinal fluid (CSF) or white matter tissue within the predominantly gray matter regions defined by the AAL atlas were not masked by each subject's anatomical MRI.

Functional Connectivity.   Average time series were extracted for each subject from 600 anatomical regions of interest (ROIs) defined by an upsampled version of the AAL atlas [13] covering the whole brain and including cortical and subcortical regions but excluding the cerebellar regions and vermis (see subsequent section on 'Atlases and Upsampling Procedure'). We focused our investigation on low frequency (0.06-0.125 Hz) oscillations in the BOLD signal that have previously been shown to support both resting [5, 3] and task-based connectivity [6]. The frequency band of interest was isolated by applying the maximal overlap discrete wavelet transform to each time series [14] and selecting scale 2 wavelet coefficients. Given TR=2s, scale 2 coefficients correspond approximately to the frequency range of interest. We estimated the functional connectivity by computing the absolute value of the Pearson's correlation between all possible pairs of time series, creating a 600×600 (M×M) connectivity matrix. Task-driven connectivity estimates were computed over the entire time series (240 and 540 volumes for attention and memory scans, respectively), consistent with previous studies [15, 16, 17].

Structural Connectivity

Diffusion Data Preprocessing.   Data preprocessing and tractography were consistent with that reported in [18]. Motion artifact and image distortions caused by eddy-currents were corrected in FMRIB's Diffusion Toolbox in FSL software by applying an affine alignment of each diffusion-weighted image to the $b0$ image. In the current study, we did not correct for EPI distortions. In this Siemens scanner, the geometric distortion for diffusion imaging from EPI was found in prior tests to be less than 2mm (i.e., less than a single voxel) and was identified primarily along the anterior posterior (phase encoding) direction. Because the resolution of the diffusion images was larger than the magnitude of the distortion, no correction was required.

Tractography.   Reconstruction of the diffusion images was performed using Diffusion Toolkit (DTK) (Ruopeng Wang, Van J. Wedeen, TrackVis.org, Martinos Center for Biomedical Imaging, Massachusetts General Hospital (MGH) [19]), a recently constructed software toolbox that provides precise diffusion imaging analysis and visualization capabilities [20, 21, 22, 23, 24, 25]. Diffusion tensor estimation was performed using the linear least-squares fitting method [19]. Raw data was not smoothed or sharpened prior to reconstruction. Deterministic tractography was subsequently performed in TrackVis software using the Fiber Assignment by Continuous Tracking (FACT) algorithm [26, 27, 28]. In this process, a single seed was placed in the center of each voxel, and the path was continued into the adjacent voxel that minimized the path curvature. Paths were terminated for curvatures greater than 35°. Fiber tracts that were rejected by the algorithm, such as those rejected due to high curvature, were not included in the present analysis. No further parameter tuning was performed within the software toolbox. Importantly, in using DTK, we performed an exhaustive search approach in which fiber tracking was performed within all voxels rather than within a set of regions specified *a priori*. Inter-regional connectivity was then examined by applying a set of gray matter masks to the complete tractography solution and by quantifying the number and length of tracts that passed between any two masks.

Inter-regional Connectivity.   In order to attain regional, rather than voxel-based, connectivity estimates, a set of M brain region masks were applied to the reconstructed fiber tracts using the UCLA Multimodal Connectivity Package (UMCP). We extracted two separate regional connectivity matrices: the total number and average length, as defined below.

For all possible pairs of M masks, we determined the number of tracks originating in mask i and terminating in mask j ($i \neq j$), thereby creating an $M \times M$ inter-regional anatomical connectivity matrix, N, where each element N_{ij} specifies the number of tracts originating in mask i and terminating in mask j. The matrix sum of the connectivity matrix is the total number of reconstructed fiber tracts, F, between grey matter masks: $F = \sum_{i \neq j} N_{ij}$. The number of fiber tracts F uncovered by the algorithm was data driven rather that defined *a priori* and was therefore variable from subject to subject. In addition to the connectivity matrix, we determined the tract length matrix, L, where each element L_{ij} specifies the average length of the tracts originating in mask i and terminating in mask j.

Cortical Parcellation

Brain Region Masks

Masks for each of the M regions of a cortical atlas were transformed into the subject's native space in a multi-step process [29, 30]. The subject's MPRAGE scans from the three sessions were averaged together to create a mean structural scan, which was then registered to the subject's $b0$ diffusion image using the affine transform provided by FSL's linear registration toolbox, FLIRT. This native space MPRAGE was then registered to the nonlinear MNI 152 T1 2mm brain. The inverse of this transformation matrix was then used to warp the atlas ROIs into subject-specific native space. The use of the MPRAGE as an intermediary between the native space and MNI space significantly increased registration fidelity and reproducibility of subsequently measured network properties.

Atlases and Upsampling Procedure

We employed an upsampled version of the original Automated Anatomical Labeling Atlas (AAL) [13, 31] containing 90 cortical and subcortical regions of interest but not containing cerebellar structures or the brainstem. This resampled version contained 600 regions of interest and was created via a series of upsampling steps in which any given region was bisected perpendicular to its principal spatial axis in order to create 2 equally sized sub-regions. Larger and smaller AAL regions were respectively upsampled more less and less in an effort to create an atlas of roughly equally-sized regions that still obeyed gross anatomical boundaries. The final atlas contained regions of an average size of 268 voxels (with a standard deviation of 35 voxels).

Our choice of atlases was motivated by current work in the field. Several recent studies have highlighted the effect of region size on structural connectivity estimates [32, 18]. These results suggest that findings drawn from whole-brain atlases with highly variable region size must be interpreted carefully. One alternative approach is to employ a parcellation scheme of identically-sizes regions placed in a grid-like fashion across the brain (e.g. [33]). However, this approach selects regions of interest that can lie across important anatomical boundaries such as gyri and sulci. To address this issue, we have chosen to create an atlas of 600 regions with roughly uniform size, none of which cross the anatomical boundaries specified by the original AAL atlas. Regions within our 'uniform-600' atlas are therefore approximately equal in size while remaining anatomically constrained.

RESULTS

Overview

In the main text, we assessed the strength of structural and functional connectivity (SC and FC, respectively) between the 600 brain regions within the uniform-600 atlas. The strength of SC between regions i and j was defined by the matrix elements L_{ij} and N_{ij} of the connectivity matrices defined in the previous section (see 'Inter-regional Connectivity'). Qualitatively similar results were obtained by rescaling $N \rightarrow N/L$, a method that was previously suggested to account for bias in the tractography algorithm [32], and we therefore report results using the direct measure N. The strength of FC was defined by BOLD correlations as described in the previous sections (see 'Functional Connectivity') and was separately assessed at rest (rsFC), in deviations ΔasFC = asFC − rsFC of the attention state (asFC) from rest, and in deviations ΔmsFC = msFC − rsFC of the memory state (msFC) from rest. The memory state was defined in the main text to be the strength of deviations ΔmsFC measured during the faces memory task. We later compare within this supplement the strength of ΔmsFC measured during the faces memory task versus the words memory task.

By relating these structural and functional connectivity measures, we examined the extent to which (i) functional connectivity could be inferred from structural connectivity (SC → FC) and (ii) structural connectivity could in turn be inferred from functional connectivity (FC → SC). We assessed these relationships within subject-averaged, or "representative", brain networks, for which the average strength of connectivity $\langle O_{ij} \rangle_s$ between regions i and j is given by:

$$\langle O_{ij} \rangle_s = \frac{1}{N_s} \sum_{s=1}^{N_s} O_{ij}^s, \tag{0.1}$$

where $N_s = 84$ is the number of subjects and O takes on values of SC or FC. The construction of representative brain networks from subject-averaged measures of SC and FC is advantageous for identifying structure-function relationships that are common to many subjects, which can then be compared to structure-function relationships observed within subject-specific brain networks. In comparing connectivity measures across subjects, we computed subject-specific connectivity strengths $\langle O \rangle_c$ as averages across connections within a single subject:

$$\langle O \rangle_c = \frac{1}{N_c} \sum_{i,j}^{N_c} O_{ij}, \tag{0.2}$$

where N_c gives the number of region pairs used in the analysis, with $N_c = 3079$ for the analysis of SC $\rightarrow$ FC, and $N_c = 3079$ for the analysis of FC $\rightarrow$ SC.

The regions pairs selected for each analysis were chosen based on their likelihood of being consistently structurally connected across a large percentage of subjects. To measure this consistency, we defined the subject-specific binary quantity C, such that $C_{ij} = 1$ if regions i and j are connected by one or more white matter tracts within a single subject, and $C_{ij} = 0$ otherwise. We defined the consistency of connectivity to be the subject-averaged quantity $\langle C_{ij} \rangle_s$, which specifies the fraction of subjects that show one or more white matter tracts linking regions i and j (e.g. a value of $\langle C_{ij} \rangle_s = .75$ indicates that regions i and j are linked by one or more structural connections within 75% of subjects).

Because the consistency $\langle C_{ij} \rangle_s$ does not have an analogously continuous subject-specific correlate (but rather has only the binary correlate C), and because the computation of $\langle C_{ij} \rangle_s$ inherently requires the use of structural information, we identified two additional measures that relate to this consistency. Importantly, these measures (one structural and one nonstructural) can be defined as subject-averaged or subject-specific quantities, enabling the comparison between representative and subject-specific brain networks. Furthermore, the use of a structural measure to select regions for the inference of function does not make any *a priori* assumptions about functional information, nor does the use of a nonstructural measure to select regions for the inference of structure make any *a priori* assumptions about structural information. These measures are defined as follows:

The rescaled number of connections $\bar{N}_{ij}$ between regions i and j, given by:

$$\bar{N}_{ij} = \frac{\langle N_{ij} \rangle_s}{\sigma_s(N_{ij})}, \tag{0.3}$$

is a purely structural measure that assesses the reliability in connection number across subjects. The denominator of this quantity gives the standard deviation in number $\sigma_s(N_{ij})$ computed across subjects:

$$\sigma_s(N_{ij}) = \sqrt{\frac{1}{N_s} \sum_s^{N_s} \left(N_{ij}^s - \langle N_{ij} \rangle_s \right)^2}. \tag{0.4}$$

We additionally specify the purely nonstructural measure of inverse interregional distance $1/d_{ij}$, defined by the metric distance d_{ij} between the center of mass positions (x, y, z) of regions i and j:

$$\frac{1}{d_{ij}} = \frac{1}{\sqrt{(x_i - x_j)^2 + (y_i - y_j)^2 + (z_i - z_j)^2}} \tag{0.5}$$

In the main text, we showed that increasing values of both $\bar{N}$ and $1/d$ relate to increasing values of the consistency $\langle C \rangle_s$. We therefore say that $\bar{N}$ and $1/d$ are indirect measures of consistency, while $\langle C \rangle_s$ is, by our definition, the direct measure of consistency. The dependence of $\langle C \rangle_s$ on $\bar{N}$ and $1/d$ enables us to isolate region pairs that are consistently structurally-connected (high values of $\langle C \rangle_s$) by selecting region pairs above the threshold values $\bar{N}_T = 0.6$ and $1/d_T = 0.1$mm. From the set of region pairs selected via $\bar{N}_T$ and $1/d_T$, we constructed two representative brain networks for the separate assessment of (*i*) SC $\rightarrow$ FC and (*ii*) FC $\rightarrow$ SC.

In (*i*), we imposed a length threshold $L_T = 20$mm to separate short ($L \leq L_T$) from long ($L > L_T$) connections, and we imposed a number threshold $N_T = 30$ to separate dense ($N > N_T$) from sparse ($N \leq N_T$) connections. Note that our use of the terms "dense" and "sparse" to refer to high and low connection numbers differs from definitions of density in which the number of tracts is scaled by the total cross sectional tract area (e.g. [32]). In combination with the separate consideration of inter- and intra-hemispheric connections, these partitions in length and number define four non-overlapping structural subgroups: short and long inter-hemispheric connections, and short but dense and long but sparse intra-hemispheric connections, whose functional properties we compared to the remaining bulk of short, sparse intra-hemispheric connections. In Figure 2 of the main text, we showed that these structural subgroups were indicative of shifts in the strength of rsFC, ΔasFC, and ΔmsFC observed within representative and subject-specific brain networks.

As the resting state was shown to exhibit the most pronounced separation in the functional properties of structural subgroups, we used resting state FC, rather than task-driven FC, to infer underlying structural properties in (*ii*). We imposed two functional thresholds rmFC_T to partition region pairs into three equal-sized functional subgroups

that show weak (bottom 33%), intermediate (mid 33%), and strong (top 33%) rsFC. We showed that these functional subgroups were supported by structural connections that differed in both length and number.

In what follows, we address four specific points of this analysis. (1) We identify the anatomical regions that participate in the structural subgroups whose regions were selected via $\bar{N}_T$ and partitioned via L_T and N_T, and similarly those regions that participate in the functional subgroups whose regions were selected via $1/d_T$ and partitioned via rsFC$_T$. (2) We show that our results are robust to variations in the selection of regions via $\bar{N}_T$ and $1/d_T$ (versus the selection via thresholds $\langle C \rangle_T$ in the direct consistency $\langle C \rangle_s$) and to variations in the structural and functional partitions imposed by L_T, N_T, and rsFC$_T$. (3) We compare the results of using memory-state connectivity msFC measured from the faces memory task versus the words memory task. (4) We discuss the extent to which variability in the consistency of structural connectivity, introduced by the selection of region pairs via $\bar{N}$ and $1/d$, impacts the results discussed here and in the main text.

Anatomical Regions Involved in Structural and Functional Subgroups

The analysis in the main text assessed structural and functional connectivity between regions within the uniform-600 atlas. As described in the previous section (see 'Atlases and Upsampling Procedure'), each of the 600 regions of interest (denoted here by ROI$_{600}$) is upsampled from and therefore fully contained within a specific anatomical region within the AAL atlas [13] (denoted ROI$_{90}$). As a result, we can map each ROI$_{600}$ to the corresponding anatomical region ROI$_{90}$ from which it was upsampled. This enables us to tabulate the specific anatomical regions that participate in the structural and functional subgroups assessed in the main text and described in the overview above.

Figures S1 and S2 show the observed connectivity patterns between ROI$_{90}$ pairs, where alternating rows and columns indicate the same anatomical regions in the right versus left hemispheres. Highlighted squares indicate that one or more ROI$_{600}$ contained within the given ROI$_{90}$ participates in the respective structural or functional subgroup.

Inspection of Figure S1 shows that the brain is sparsely connected, exhibiting only a small fraction of all possible structural connections between brain regions. Dense intra-hemispheric connections tend to self-connect single anatomical regions and interconnect regions within the same anatomical lobe, as is observed by the block-diagonal groupings in Figure S1. In comparison, long intra-hemispheric connections, occupying off-diagonal elements in Figure S1, commonly link distant regions in distinct anatomical lobes and are largely found between subcortical and frontal regions and between limbic and occipital regions. Short and long inter-hemispheric regions tend to be clustered together to link corresponding regions within the right and left hemispheres. The remaining bulk of short, sparse intra-hemispheric connections tend to link regions within the same anatomical lobe.

The functional properties of the regions linked by these structural connections show similar anatomical organization (Figure S2). Regions within the same anatomical lobe tend to be strongly correlated. Regions in distinct anatomical lobes, such as those involved in connections between subcortical, frontal, and limbic regions, tend to be weakly correlated. This functional organization reflects the structural organization of, for example, dense versus long intra-hemispheric connections that were shown in the main text to respectively support strong versus weak resting-state correlations.

Given that the structural group of long, intra-hemispheric connections was shown in the main text to support the largest change in FC across resting and task-driven states, we separately enumerate the specific regions linked by these connections (Table 1). Examination of these regions provides insight into the observed task-dependent shifts in functional connectivity across attention and memory states, as many of the participating regions have been implicated in either visuospatial or memory processing. For example, visuospatial attention has been shown to involve activations within the superior frontal gyrus [34] and the precuneus [35] and correlated activations between the right thalamus and the right caudate nucleus [36]. Memory processing has been shown to involve the hippocampus, the right caudate nucleus, and the middle temporal gyrus [37, 38], and patterns of connectivity between these regions are thought to play important roles in memory-related functional networks [39]. Other regions, including the anterior and posterior cingulate, have been linked to both visuospatial processing [40] and self-referential processing [41].

Robustness to Thresholding

In selecting and partitioning groups of region pairs for the construction of brain networks, we made specific choices about both the number of retained region pairs and the divisions used to group connections between these region pairs. In what follows, we evaluate the structural and functional connectivity of the representative brain networks across variations in the thresholds used to construct ($\bar{N}_T$ and $1/d_T$) and partition (L_T, N_T, and rsFC$_T$) these networks. We assess this robustness to thresholding within our two analyses, SC → FC and FC → SC, and we show that the correlations between structure and function observed in each analysis are robust to thresholding.
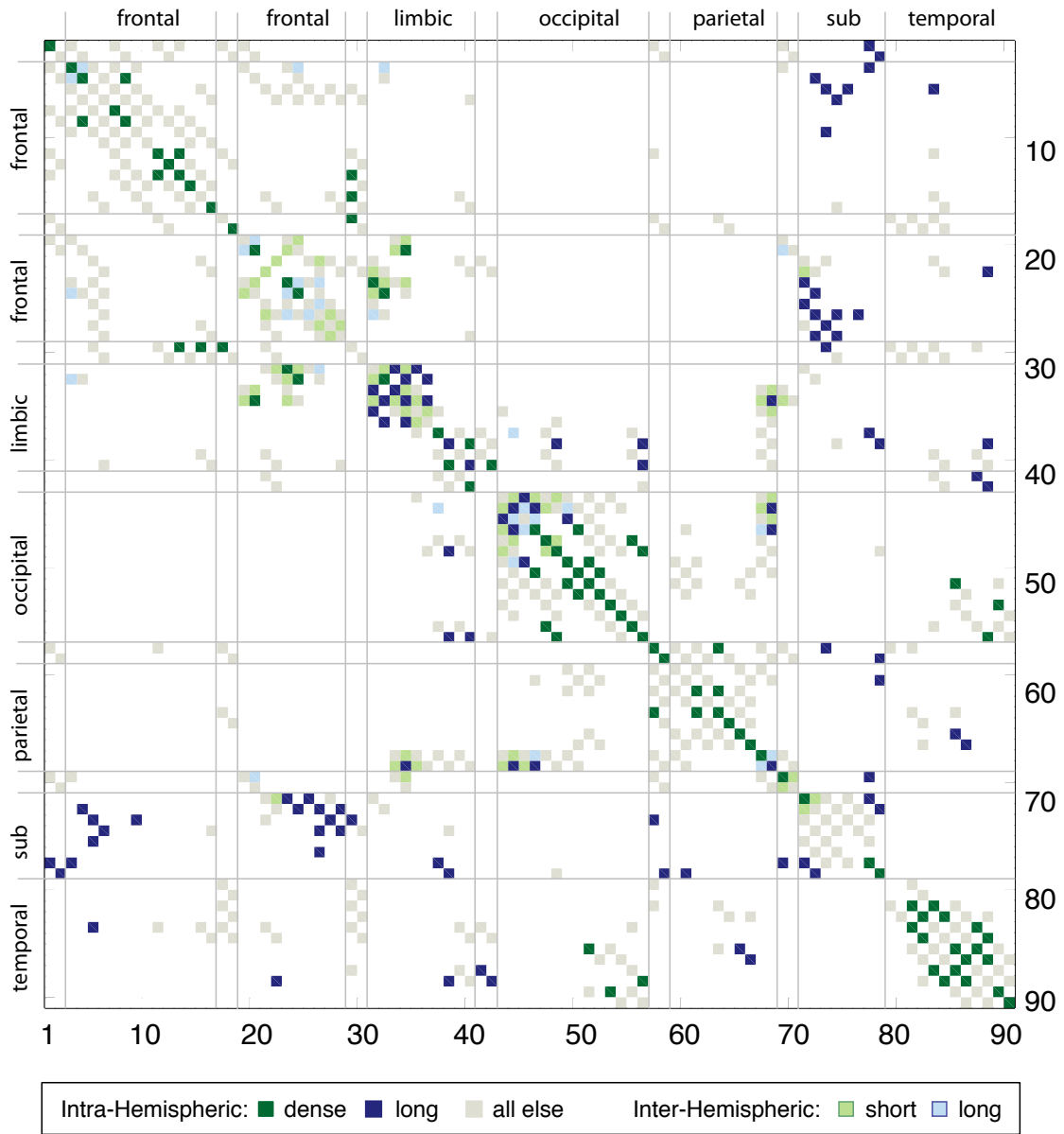
Figure S1: **Anatomical Regions Linked by Structural Subgroups.** Regions are numbered according to their label in the 90-region AAL atlas, with odd and even numbers respectively indicating regions within left and right hemispheres. Horizontal and vertical lines delineate the following anatomical groupings: frontal lobe, limbic lobe, occipital lobe, parietal lobe, subcortical regions, and temporal lobe. Unlabeled regions between groupings indicate central regions, including the pre/postcentral gyri and rolandic operculum. Colored squares mark region pairs linked by different types of structural connections in the representative brain network. Structural connectivity was initially assessed between 600 regions, and these regions were then mapped to their corresponding anatomical label within the 90-region AAL atlas. Dense connections tend to lie along the diagonal, indicating that individual anatomical regions tend to be densely self-connected. Inter-hemispheric connections also tend to cluster near the diagonal to link symmetric regions between hemispheres. In comparison, long intra-hemispheric connections tend to lie far from the diagonal to link subcortical structures with other regions of the brain. The remaining bulk of short, sparse intra-hemispheric connections tend to connect different regions within the same anatomical lobe.
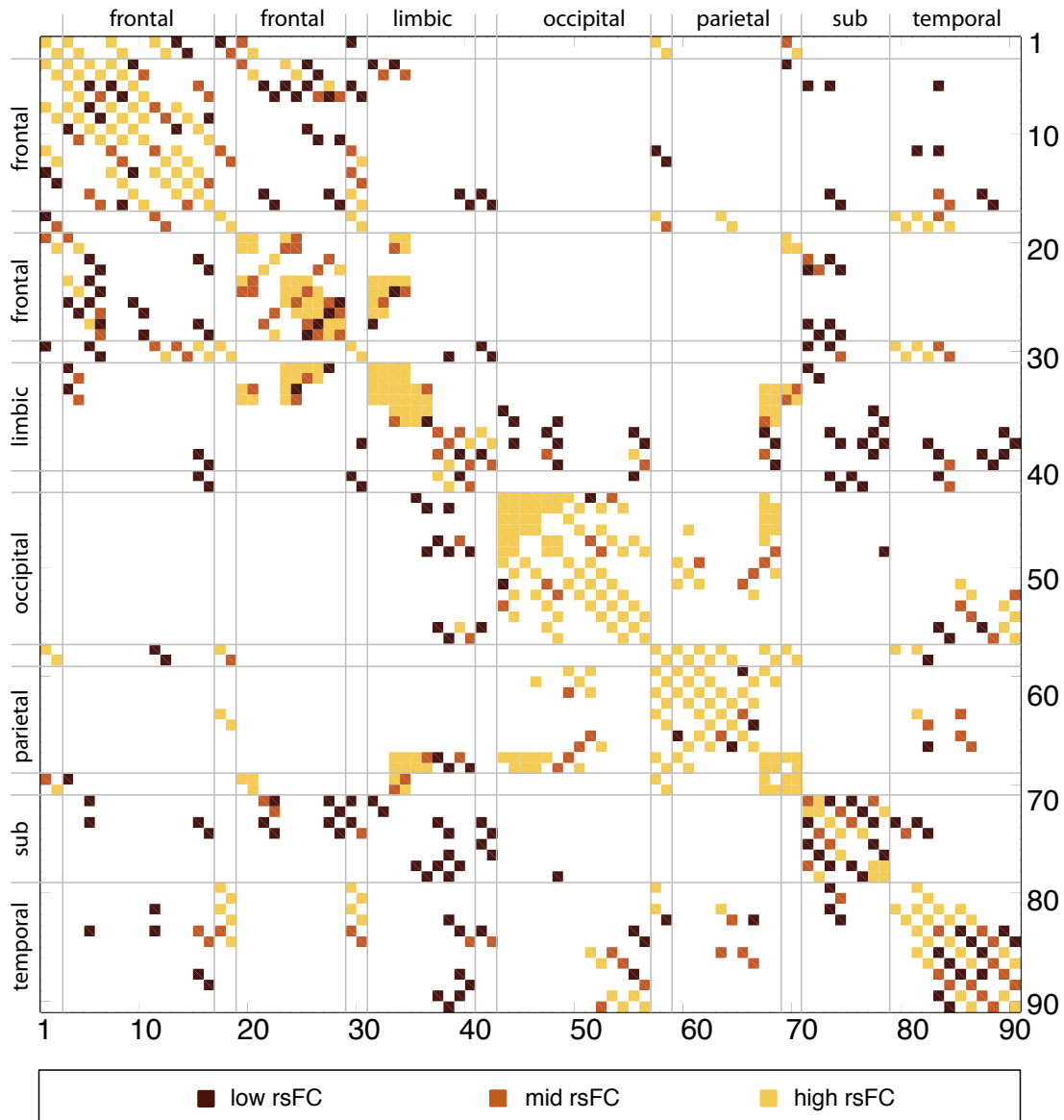
Figure S2: **Anatomical Regions Involved in Functional Subgroups.** Regions are numbered according to their label in the 90-region AAL atlas, with odd and even numbers respectively indicating regions within left and right hemispheres. Horizontal and vertical lines delineate the following anatomical groups of regions: frontal lobe, limbic lobe, occipital lobe, parietal lobe, subcortical regions, and temporal lobe. Unlabeled regions between groupings indicate central regions, including the pre/postcentral gyri and rolandic operculum. Colored squares mark region pairs involved in different functional connections within the representative brain network. Functional connectivity was initially assessed between 600 regions, and these regions were then mapped to their corresponding anatomical label within the 90-region AAL atlas. Note that, because the region pairs used to infer SC from FC were selected via different measures than the regions used to infer FC from SC, the region pairs shown here largely overlap with, but are not identical to, the set of regions shown in Figure S1. Strongly-correlated region pairs tend to be clustered along the diagonal and tend to dominate the connections within frontal, occipital, and parietal regions, while weakly-correlated region pairs tend to dominate off-diagonal connections between subcortical, frontal, and limbic regions.

Table 1: **Anatomical Regions Linked by Long, Intra-Hemispheric Connections.** Shown are anatomical regions in the 90-region AAL atlas that are linked by long intra-hemispheric connections. We differentiate between connections within a given anatomical region from those that link two different anatomical regions. The number of region pairs involved in connections within the right (R) and left (L) hemispheres in indicated in the rightmost column.

| **Within Regions**		**# R (L)**
Hippocampus		2(0)
Parahippocampal gyrus		1(0)
Calcarine		2(0)
Precuneus		1(0)
Middle Cingulum		6(1)
Between Regions		**# R (L)**
Thalamus	Hippocampus	5(1)
	Caudate nucleus	3(1)
	Precentral gyrus	2(1)
	Paracentral lobule	0(1)
	Postcentral gyrus	1(0)
	Superior frontal gyrus, dorsolateral	0(1)
	Superior parietal gyrus	1(0)
Putamen	Superior frontal gyrus, orbital part	2(2)
	Superior frontal gyrus, medal orbital	2(0)
	Middle frontal gyrus, orbital part	0(1)
	Gyrus rectus	1(1)
	Insula	0(1)
	Postcentral gyrus	0(1)
Caudate nucleus	Superior frontal gyrus, medal orbital	3(0)
	Superior frontal gyrus, medial	1(1)
	Superior frontal gyrus, dorsolateral	1(0)
	Gyrus rectus	1(0)
Mid Cingulum	Anterior cingulate gyrus	10(1)
	Posterior cingulate gyrus	2(1)
	Precuneus	2(0)
Cuneus	Calcarine fissure	2(1)
	Precuneus	2(0)
	Superior occipital gyrus	0(1)
Hippocampus	Temporal pole, middle temporal gyrus	2(0)
	Lingual gyrus	1(0)
	Fusiform gyrus	1(0)
Temporal pole: middle temporal gyrus	Amygdala	1(1)
	Olfactory cortex	1(0)
Lenticular nucleus, pallidum	Superior frontal gyrus, orbital part	0(1)
	Superior frontal gyrus, medial orbital	1(0)
Precuneus	Calcarine fissure	2(0)
Posterior cingulate	Anterior cingulate	2(0)
Middle temporal gyrus	Angular gyrus	1(1)
Temporal pole: superior temporal gyrus	Superior frontal gyrus, orbital part	1(0)
Parahippocampal gyrus	Fusiform gyrus	1(0)
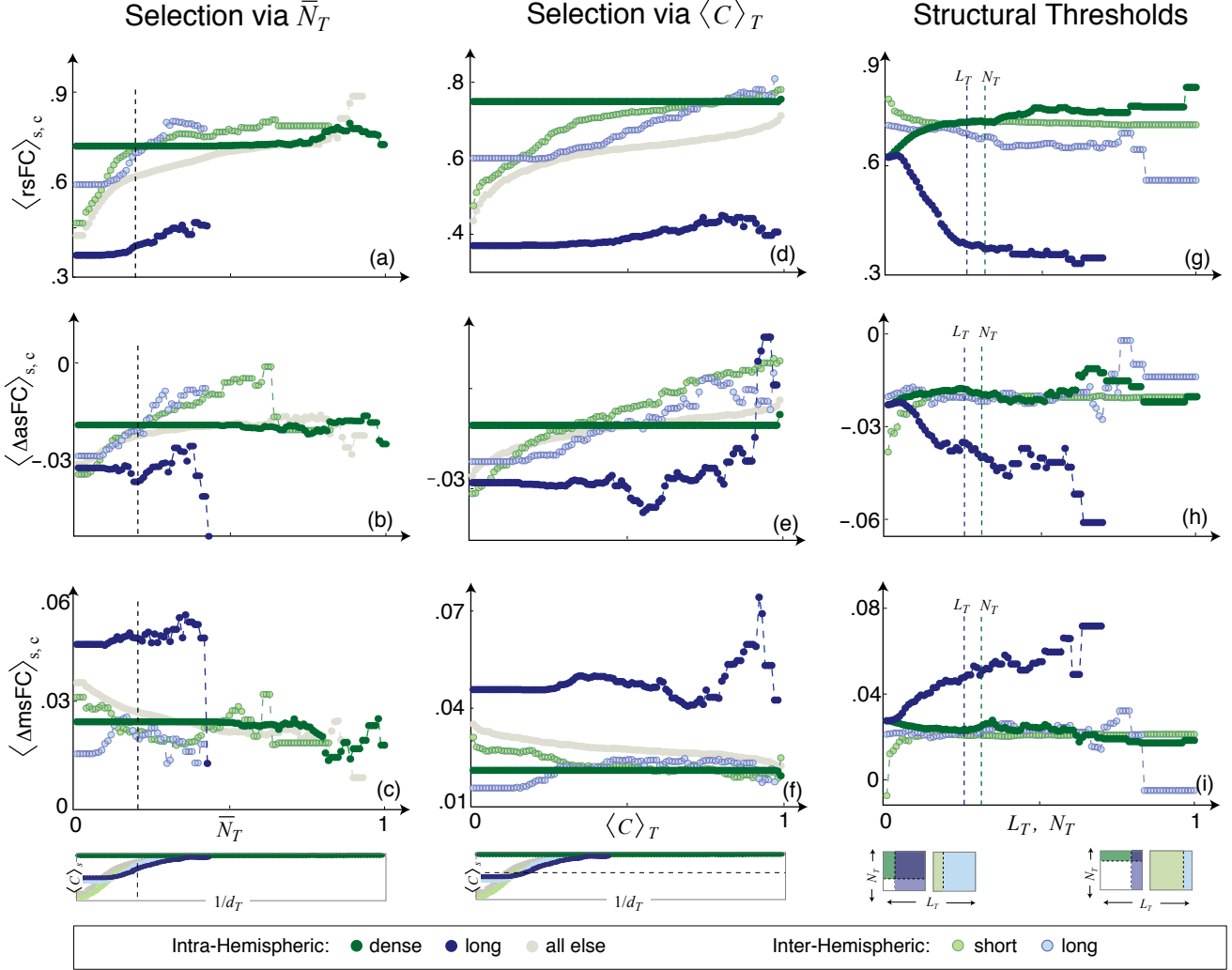
Figure S3: **Inferring FC from SC: Robustness to Thresholding.** Changes in average functional connectivity $\langle rsFC \rangle_{s,c}$, $\langle \Delta asFC \rangle_{s,c}$, and $\langle \Delta msFC \rangle_{s,c}$ produced by structural subgroups of connections across variations in the selection of regions via (a-c) $\bar{N}_T$ and (d-f) $\langle C \rangle_T$ and across variations in the (g-i) structural thresholds L_T and N_T. Thresholds are scaled by their maximum values, and the specific threshold values used in the text are indicated by dashed lines. Note that large threshold values select small numbers of region pairs and thereby introduce jitter into the distribution averages. Variations in the selection of region pairs via the indirect ($\bar{N}_T$) and direct ($\langle C \rangle_T$) measures of consistency produce similar shifts in $\langle FC \rangle_{s,c}$ that collectively increase with increasing threshold values. In comparison, variations in structural thresholds alter the separation in $\langle FC \rangle_{s,c}$ across structural subgroups. All threshold variations maintain consistent relationships between SC and FC to those observed in the main text. Structural subgroups show the most pronounced separation in $\langle FC \rangle_{s,c}$ in the resting state, with inter-hemispheric and dense intra-hemispheric connections producing consistently strong $\langle rsFC \rangle_{s,c}$ and long intra-hemispheric connections producing consistently weak $\langle rsFC \rangle_{s,c}$ (top row). During task performance, inter-hemispheric and dense intra-hemispheric connections produce similar changes in $\langle FC \rangle_{s,c}$ to the bulk of remaining connections, while long intra-hemispheric connections producing consistently weak changes in $\langle asFC \rangle_{s,c}$ (middle row) and consistently strong changes in $\langle msFC \rangle_{s,c}$ (bottom row).

Inferring Function from Structure

The analysis of SC → FC shown in the main text was performed on a representative brain network constructed from region pairs linked by high rescaled numbers of structural connections ($\bar{N} > \bar{N}_T$). Connections between these region pairs were partitioned based on their length and number via the structural thresholds N_T and L_T. In combination with the delineation between inter- and intra-hemispheric connectivity, these partitions defined four structural subgroups, (1) short and (2) long inter-hemispheric connections, and (3) dense and (4) long intra-hemispheric connections, whose properties were compared to the remaining bulk of short, sparse intra-hemispheric connections. The subject-averaged strengths $\langle \mathrm{rsFC} \rangle_s$, $\langle \Delta\mathrm{asFC} \rangle_s$, and $\langle \Delta\mathrm{msFC} \rangle_s$ were then compared across these partitioned subgroups.

We now evaluate the robustness of structurally-dependent shifts in $\langle \mathrm{rsFC} \rangle_s$, $\langle \Delta\mathrm{asFC} \rangle_s$, and $\langle \Delta\mathrm{msFC} \rangle_s$ to variations in $\bar{N}_T$, L_T, and N_T. As a measure of comparison across thresholds, we compute the averages $\langle \mathrm{rsFC} \rangle_{s,c}$, $\langle \Delta\mathrm{asFC} \rangle_{s,c}$, and $\langle \Delta\mathrm{msFC} \rangle_{s,c}$ of the complementary cumulative distribution functions (cCDFs) produced by connections within the representative brain network. These cCDFs were shown in Figure 2d-f of the main text for the threshold values $\bar{N}_T = 0.6$, $N_T = 30$, and $L_T = 20$mm. The notation $\langle O \rangle_{s,c}$ indicates that the average of the quantity O was computed first across subjects, in constructing the representative brain network, and then across connections within the representative network. Variations in $\langle O \rangle_{s,c}$ measure relative shifts in the cCDFs across variations in thresholding.

We find that the observed shifts in FC shown in Figure 2d-f in the main text are robust to variations in thresholding, as shown here in Figure S3 and as discussed in detail below. Across all threshold values, inter-hemispheric FC shows minimal dependence on connection length, with both short and long inter-hemispheric connections supporting strong rsFC and similar changes in asFC and msFC to the remaining bulk of connections. Dense intra-hemispheric connections show nearly consistent FC strength across thresholding scenarios, exhibiting notably strong rsFC. Long intra-hemispheric connections consistently show task-dependent changes in FC, exhibiting low values of rsFC, decreases in asFC from rest, and increases in msFC from rest.

Variations in Selection Thresholds. Increasing the selection threshold $\bar{N}_T$ corresponds to retaining fewer region pairs that are more densely connected across subjects (left column of Figure S3). As mentioned previously (see 'Results: Overview'), $\bar{N}$ is an indirect measure of the consistency in connectivity $\langle C \rangle_s$, and therefore the densely-connected region pairs selected via $\bar{N}_T$ also tend to be consistently connected within a large fraction of subjects. The selection of region pairs via $\bar{N}$, rather than via $\langle C \rangle_s$, is advantageous because $\bar{N} = \langle N \rangle_s / \sigma_s(N)$ has an analogous single-subject correlate given by the number of connections N scaled by the uncertainty in the measurement of N. In comparison, the single-subject correlate of the measure $\langle C \rangle_s$ is the subject-specific binary number C, which cannot be used as a continuous threshold for region pair selection.

To confirm that region pair selection via $\bar{N}_T$ produces similar results to region pair selection via $\langle C \rangle_s$, we compare shifts in $\langle \mathrm{rsFC} \rangle_{s,c}$, $\langle \Delta\mathrm{asFC} \rangle_{s,c}$, and $\langle \Delta\mathrm{msFC} \rangle_{s,c}$ across variations in both $\bar{N}_T$ and $\langle C \rangle_T$, shown respectively in the left and middle columns of Figure S3.

Because $\bar{N}$ scales with the consistency $\langle C \rangle_s$, and because the distributions of $\langle \mathrm{FC} \rangle_s$ are insensitive to inconsistent connectivity (see later section on 'Inconsistent Connectivity in the Representative Brain'), variations across $\bar{N}_T$ and $\langle C \rangle_T$ produce similar results, with the latter producing stronger separations in FC across structural groups (middle column of Figure S3). For both choices of selection threshold, the overall strength $\langle \mathrm{FC} \rangle_{s,c}$ increases with increasing threshold.

Variations in Structural Thresholds. Variations in the structural thresholds L_T and N_T alter the partitioning of connections into long ($L > L_T$) versus short ($L \leq L_T$) and dense ($N > N_T$) versus sparse ($N \leq N_T$) subgroups, which in turn alter the degree of separation in FC observed across structural subgroups.

Biasing toward higher numbers of connections (by increasing N_T) increases the strength of $\langle \mathrm{FC} \rangle_{s,c}$ in the resting state but has a limited effect on task-driven states, producing a slight increase in $\langle \Delta\mathrm{asFC} \rangle_{s,c}$ and a slight decrease in $\langle \Delta\mathrm{msFC} \rangle_{s,c}$. Biasing toward longer connections (by increasing L_T) increases the separation in $\langle \mathrm{FC} \rangle_{s,c}$ between short and long inter- and intra-hemispheric connections. The separation in inter-hemispheric $\langle \mathrm{FC} \rangle_{s,c}$, however, is consistently smaller than the separation in intra-hemispheric $\langle \mathrm{FC} \rangle_{s,c}$. Most notably, biasing toward longer connections reveals that long intra-hemispheric connections show increasingly weak $\langle \mathrm{FC} \rangle_{s,c}$ in the resting and attention states and increasingly strong $\langle \mathrm{FC} \rangle_{s,c}$ in the memory state, thereby confirming that the task-dependent shifts observed in Figure 2d-f in the main text are not artifacts of thresholding.

Inferring Structure from Function

The analysis of FC → SC shown in the main text was performed on a representative brain network constructed from region pairs within close interregional distances ($1/d > 1/d_T$). Region pairs were partitioned based on their strength of rsFC via the functional thresholds rsFC_T into three functional groups exhibiting (1) weak (bottom 33%), (2)
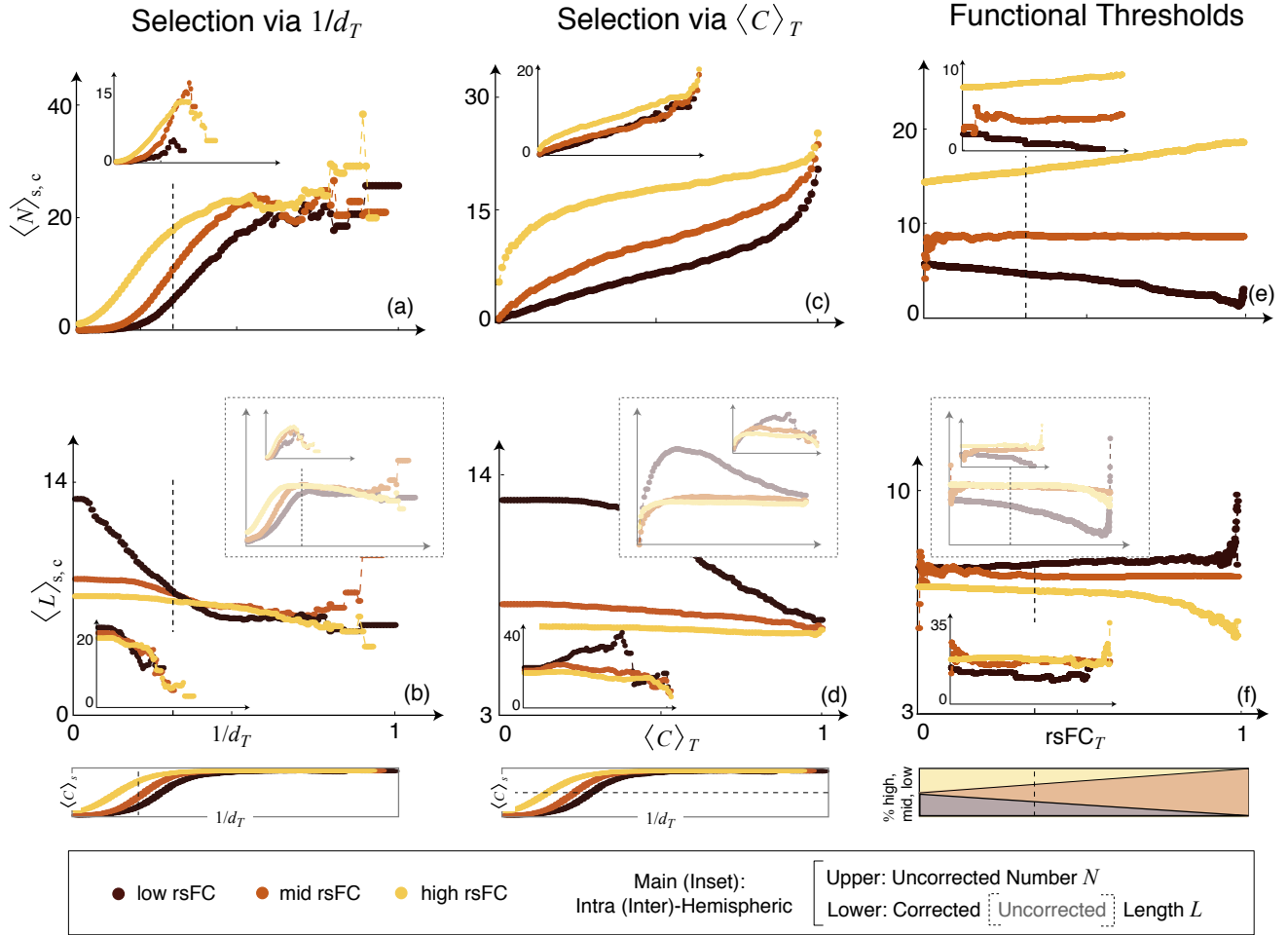
Figure S4: **Inferring SC from FC: Robustness to Thresholding** Changes in average structural measures $\langle N \rangle_{s,c}$ and $\langle L \rangle_{s,c}$ produced by functional subgroups of connections across variations in the selection of regions via (a-c) $1/d_T$ and (d-f) $\langle C \rangle_T$ and across variations in the (g-i) functional thresholds rsFC$_T$, with inter-hemispheric values shown in insets. Thresholds are scaled by their maximum values, and the specific threshold values used in the text are indicated by dashed lines. The corrected length distributions, for which connections with unphysical lengths have been removed, are shown in the lower row of the figure, with the uncorrected distributions shown across identical scales within the dotted insets. Variations in the selection of region pairs via the indirect ($1/d_T$) and direct ($\langle C \rangle_T$) measures of consistency produce similar shifts in $\langle SC \rangle_{s,c}$, with the overall values of $\langle N \rangle_{s,c}$ and $\langle L \rangle_{s,c}$ tending to respectively increase and decrease with increasing threshold values. In comparison, variations in the functional thresholds alter the separation in $\langle N \rangle_{s,c}$ and $\langle L \rangle_{s,c}$ across functional subgroups. All threshold variations maintain consistent relationships between SC and FC to those observed in the main text, with shorter intra-hemispheric connection lengths and higher numbers of inter- and intra-hemispheric connections consistently supporting strong rsFC. Inspection of the uncorrected values of $\langle L \rangle_{s,c}$ reveals that the relationship between increasingly short intra-hemispheric connections and increasingly strong rsFC can be recovered if (b) unphysical connection lengths selected via $1/d_T$ are separately removed, if (d) regions are selected via $\langle C \rangle_T$ such that the inconsistent connections that give rise to unphysical connection lengths are automatically removed, or if (f) the functional thresholds rsFC$_T$ are tuned to select very strongly- and very weakly-correlated region pairs.

16

intermediate (middle 33%), and (3) strong (top 33%) rsFC. These subgroups were further delineated into inter- and intra-hemispheric functional groups. The subject-averaged structural properties $\langle L \rangle_s$ and $\langle N \rangle_s$ were then compared across these partitioned subgroups.

We now evaluate the robustness of functionally-dependent shifts in $\langle L \rangle_s$ and $\langle N \rangle_s$ to variations in $1/d_T$ and $\mathrm{rsFC_T}$. As a measure of comparison across thresholds, we compute the averages $\langle L \rangle_{s,c}$ and $\langle N \rangle_{s,c}$ of the cCDFs produced by connections within the representative brain network. These cCDFs were shown in Figure 3c-d of the main text for the threshold values $1/d_T = 0.1$ and $\mathrm{rsFC_T} = 1/3$.

We find that the observed shifts in SC shown in Figure 3c-d in the main text are robust to variations in thresholding, as shown here in Figure S4 and as discussed in detail below. Across all threshold variations, high numbers of inter- and intra-hemispheric connections consistently support strong rsFC. In assessing the distributions of connection lengths, which are shown in a later section to be sensitive to the presence of connections with unphysical connection lengths, we separately consider the uncorrected (dotted insets) and corrected (main figure) distributions for which connections with unphysical lengths are respectively included or excluded. The corrected distributions show that short intra-hemispheric connection lengths consistently support strong rsFC. A thorough discussion of the identification and implications of unphysical connections can be found in the later section entitled 'Inconsistent Connectivity in the Representative Brain Network'.

Variations in Selection Thresholds. Increasing the selection threshold $1/d_T$ corresponds to retaining region pairs that are closer in physical proximity (left column of Figure S4). As mentioned previously, $1/d$ is an indirect measure of the consistency in connectivity $\langle C \rangle_s$, and therefore region pairs in close physical proximity also tend to be consistently connected within a large fraction of subjects. The selection of region pairs via $1/d$, rather than via $\langle C \rangle_s$, is advantageous because $1/d$ does not rely on knowledge of anatomical connectivity and therefore does not suffer from the circular use of structural information for the inference of structural information. In comparison, the measure $\langle C \rangle_s$ relies on knowledge of the presence or absence of structural connectivity between region pairs.

To confirm that region pair selection via $1/d_T$ produces similar results to region pair selection via $\langle C \rangle_s$, we compare shifts in $\langle N \rangle_{s,c}$ and $\langle L \rangle_{s,c}$ across variations in both $1/d_T$ and $\langle C \rangle_T$, shown respectively in the left and middle columns of Figure S4.

Because $1/d$ scales with the consistency $\langle C \rangle_s$, and because the distribution of $\langle N \rangle_s$ is insensitive to inconsistent connectivity (discussed in the following section), variations across $1/d_T$ and $\langle C \rangle_T$ produce similar distributions of connection numbers, with the latter producing a more pronounced separation in the large number of inter- and intra-hemispheric connections that support strong versus weak correlations (middle column of Figure S3). Increases in both threshold values result in an overall increase in connection number.

In comparison to the distribution of $\langle N \rangle_s$, the distribution of $\langle L \rangle_s$ varies depending on whether regions are selected via $1/d_T$ or $\langle C \rangle_T$, and whether connections with unphysical lengths are included in or excluded from the analysis. When unphysical connections are excluded (Figure S4b,d), variations in both $1/d_T$ and $\langle C \rangle_T$ produce consistent results, with increasingly short intra- and inter-hemispheric connections supporting increasingly strong rsFC. Region selection via $\langle C \rangle_T$ produces a stronger separation in the length of inter- and intra-hemispheric connections that support strong versus weak rsFC, as was similarly observed in the distributions of connection numbers. Increases in both threshold values result in an overall decrease in the average connection length.

When unphysical connections are included, however, variations in $1/d_T$ and $\langle C \rangle_T$ produce different results (dotted insets in Figure S4b,d). Region selection via $1/d$ shows that strongly-correlated regions are linked by longer, rather than shorter, intra- and inter-hemispheric connections. Region selection via $\langle C \rangle_s$ recovers the relationship between short intra- and inter-hemispheric connection length and strong rsFC, confirming that inconsistency in connectivity (quantified by low values of $\langle C \rangle_s$) are responsible for the altered relationship between connection length and rsFC strength.

Regardless of the selection of regions via $1/d$ versus $\langle C \rangle_s$, and regardless of whether unphysical connections are included in or excluded from the analysis, the distributions of inter-hemispheric connection lengths show much less separation across functional subgroups than do the distributions of intra-hemispheric connection lengths.

Variations in Functional Thresholds. Variations in the functional threshold $\mathrm{rsFC_T}$ shift the delineations between region pairs that exhibit weak, intermediate, and strong rsFC (right column of Figure S4). We vary this threshold such that the strongly- and weakly-correlated groups consist of the same number of region pairs but can differ in number from the intermediate group, such that the strongly- and weakly-correlated groups are highly populated for small values of $\mathrm{rsFC_T}$, while the intermediate group is highly populated for large values of $\mathrm{rsFC_T}$. Variations in functional threshold values alter the observed separation in SC across functional subgroups.

Biasing toward very strong and very weak rsFC by increasing $\mathrm{rsFC_T}$ in turn increases the separation in the number of connections that support strong versus weak rsFC, with high numbers of inter- and intra-hemispheric connections

consistently supporting strong rsFC (Figure S4e).

The impact of variations in rsFC_T on the distribution of connection lengths depends on the inclusion versus exclusion of connections with unphysical lengths (main portion versus dotted inset of Figure S4f). When unphysical connections are excluded from the analysis, variations in rsFC_T increase the separation in the length of connections that support strong versus weak rsFC, with short intra-hemispheric connections consistently supporting strong rsFC. When unphysical connections are included in the analysis, however, strong rsFC appears to be supported by longer, rather than shorter, intra-hemispheric connections across variations in rsFC_T. In both cases, stronger inter-hemispheric rsFC is supported by slightly longer, rather than shorter, connections. The observed separation in length across functional subgroups, however, is much less pronounced for inter- versus intra-hemispheric connections.

Considerations for Inter- versus Intra-Hemispheric Connections. Because inter- and intra-hemispheric connections differ in their structural properties, their distributions of SC show different sensitivities to variations in threshold values and to the inclusion versus exclusion of connections with unphysical lengths.

Relatively few inter-hemispheric regions are linked by connections with unphysical lengths (see later sections on 'Inconsistent Connectivity in the Representative Brain Network'), and therefore the distributions of inter-hemispheric number and length are less sensitive to the exclusion of unphysical connections than are intra-hemispheric distributions. Regardless of whether unphysical connections are included in or excluded from the analysis, inter-hemispheric regions are consistently linked by fewer connection numbers and greater connection lengths, on average, than intra-hemispheric regions, a trend that is maintained across variations in all threshold values. In contrast to the consistently large separation in SC observed between intra-hemispheric functional subgroups, inter-hemispheric subgroups show reduced separation in the structural properties that support strong versus weak correlations. Furthermore, the relative contribution from long versus short inter-hemispheric connections is variable across thresholding scenarios. Together, these results provide additional support for our previous finding that the functional correlations between inter-hemispheric regions are less sensitive to underlying structure than are functional correlations between intra-hemispheric regions.

The majority of connections with unphysical lengths link intra-hemispheric regions, and therefore the distributions of intra-hemispheric connection length (but not number; see 'Inconsistent Connectivity in the Representative Brain Network') are sensitive to the effects of connections with unphysical length. When included in the analysis, these unphysical connections alter the apparent relationship between connection length and rsFC, such that increasingly long, rather than short, connections appear to support increasingly strong rsFC. However, large increases in functional threshold values, which bias toward the very strongest and very weakest correlations, can be used to recover the trend that short intra-hemispheric connections support strong rsFC (far right of dotted inset in Figure S4f). Importantly, this technique requires no knowledge of SC. This trend can additionally be recovered by selecting region pairs via the consistency $\langle C \rangle_s$ (dotted inset in Figure S4d). The different results obtained from the direct (via $\langle C \rangle_T$) versus indirect (via $1/d_T$) selection of consistently-connected region pairs suggests that increasing the minimum consistency, rather than the average consistency, is important for the robust inference of structure from function.

Robustness to Distance Effects

Structural and functional connectivity have both been shown in previous studies to increase in strength with decreasing interregional distance [42, 43]. To confirm that our results do not arise artificially from distance-related correlations, we relate repeat the analysis of representative brain connectivity while controlling for interregional distance.

We use an approach consistent with that described in [44]. We first verify that $\langle \text{rsFC} \rangle_s$ is linearly related to the inverse interregional distance $1/d$ ($r = .58$ and $r = .48$ for the subsets of region pairs selected via $\bar{N}_T$ and $1/d_T$, respectively). We then regress $\langle \text{rsFC} \rangle_s$ on $1/d$ to extract the residuals in $\langle \text{rsFC} \rangle_s$. Lastly, we repeat the analyses of $\text{SC} \to \text{FC}$ and $\text{FC} \to \text{SC}$ described in the main text after replacing $\langle \text{rsFC} \rangle_s$ by its residuals.

We specifically assess the separation in $\langle \text{rsFC} \rangle_s$ observed across structural subgroups (Figure 2d in the main text) and conversely the separation in $\langle N \rangle_s$ and $\langle L \rangle_s$ observed across functional subgroups (shown in Figure 3c,d in the main text). Note that, because task-dependent FC is measured in deviations from rest, regressions of $\langle \Delta \text{asFC} \rangle_s$ and $\langle \Delta \text{msFC} \rangle_s$ on $1/d$ produce nearly identical results to those shown in the main text.

Inferring Function from Structure

For the analysis of $\text{SC} \to \text{FC}$, we assess shifts in the residuals of $\langle \text{rsFC} \rangle_s$ produced by structural subgroups of connections. When distance is regressed out in this manner, we see reduced separation in $\langle \text{rsFC} \rangle_s$ across structural subgroups (Figure S5a). This is consistent with the finding that correlations between SC and rsFC are present but are weaker when controlling for distance effects [44].
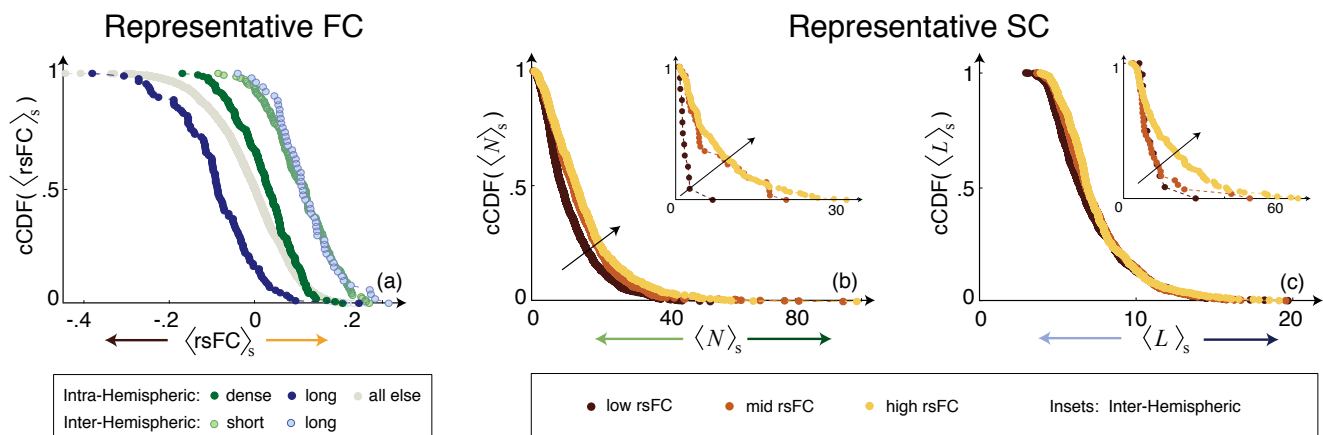
Figure S5: **Robustness of Representative SC and FC to Distance Effects.** When controlling for interregional distance, similar qualitative shifts are observed in the cCDF's of (a) $\langle \text{rsFC} \rangle_{\text{s}}$ (b) $\langle N \rangle_s$, and (c) $\langle L \rangle_s$ (corrected) produced by structural and functional subgroups of connections in the representative brain network. In all cases, the observed shifts are less pronounced when correcting for distance effects. (a) Inter-hemispheric and dense intra-hemispheric connections show stronger values of $\langle \text{rsFC} \rangle$ while long intra-hemispheric connections show weaker values of $\langle \text{rsFC} \rangle$ as compared to the remaining bulk of connections. While short and long inter-hemispheric connections show similarly strong shifts in $\langle \text{rsFC} \rangle$, the shift produced by dense intra-hemispheric connections is less pronounced. (b) Increasingly strongly correlated inter- and intra-hemispheric regions are consistently linked by higher numbers of connections. (c) Controlling for distance collapses the corrected length distributions produced by intra-hemispheric, but not inter-hemispheric, functional subgroups.

Despite the reduced separation in $\langle \text{rsFC} \rangle_{\text{s}}$ across structural subgroups, the relative shifts in $\langle \text{rsFC} \rangle_{\text{s}}$ are consistent with those observed in Figure 2d of the main text. Inter-hemispheric connections and dense intra-hemispheric connections show strong $\langle \text{rsFC} \rangle_{\text{s}}$ as compared to the remaining bulk of connections, although dense intra-hemispheric connections show less pronounced shifts in $\langle \text{rsFC} \rangle_{\text{s}}$ than do the similarly strong shifts exhibited by short and long inter-hemispheric connections. In contrast, long intra-hemispheric connections show weak $\langle \text{rsFC} \rangle_{\text{s}}$ as compared to the remaining bulk of connections.

Inferring Structure from Function

For the analysis of FC $\rightarrow$ SC, we partition the residuals of $\langle \text{rsFC} \rangle_{\text{s}}$ into functional subgroups, and we assess shifts in the number $\langle N \rangle_s$ and corrected length $\langle L \rangle_s$ of connections linking functional subgroups.

As was observed in the previous subsection, we see reduced separation in the number of connections linking functional subgroups (Figure S5b). However, the relative shifts in the number of connections linking strongly- versus weakly-correlated subgroups is consistent with the results shown in Figure 3c in the main text, with strongly-correlated inter- and intra-hemispheric regions consistently linked by higher numbers of connections.

Because intra-hemispheric connection length is closely related to interregional distance, controlling for distance removes the observed shifts in the length of connections linking intra-hemispheric functional subgroups (Figure S5c). However, because inter-hemispheric regions can be separated by short distances but linked by long connections, we see that increasingly strongly correlated inter-hemispheric regions remain consistent linked by longer connections when controlling for distance, in agreement with the results shown in Figure 3d in the main text.

Comparison of Memory for Words versus Memory for Faces

The comparison of functional connectivity across structural subgroups of connections, as assessed in the main text, compared the strength of FC measured in the resting state, during the performance of the attention task, and during the performance of the memory task for faces. Subjects also performed a memory task for words that was not assessed in the main text. Here, we show that the two memory tasks, for words and for faces, show similar shifts in the functional connectivity produced by different structural subgroups of connections. The details of the two memory tasks were described above (see Methods; Memory Tasks).

Long intra-hemispheric connections were shown in the main text to support pronounced shifts in the memory-state functional connectivity ($\langle \Delta \text{msFC} \rangle_{\text{s}}$) of the representative brain network associated with memory for faces. Here, we find that the representative brain network shows similar shifts in $\langle \Delta \text{msFC} \rangle_{\text{s}}$ associated with memory for words, with long intra-hemispheric connections supporting the largest increase in msFC among structural subgroups.
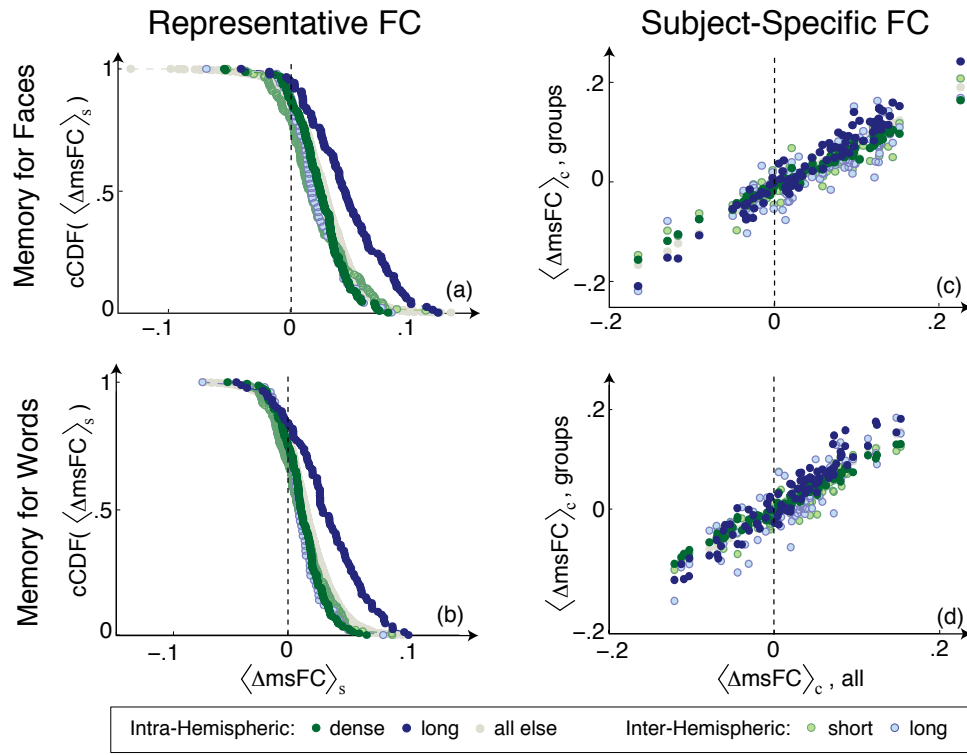
Figure S6: **Comparison of Representative and Subject-Specific FC Between Memory for Words versus Faces.** The representative brain network shows similar shifts in memory state functional connectivity ($\langle\Delta\text{msFC}\rangle_s$) between the memory tasks for (a) faces versus (b) words, with the distribution of $\langle\Delta\text{msFC}\rangle_s$ showing less variance across connections for words versus faces. For both words and faces, long intra-hemispheric connections showing pronounced shifts toward higher values of $\langle\Delta\text{msFC}\rangle_s$, while inter-hemispheric and dense intra-hemispheric connections show similar shifts in $\langle\Delta\text{msFC}\rangle_s$ to the remaining bulk of short, sparse intra-hemispheric connections. Individual subjects show similar variability in $\langle\Delta\text{msFC}\rangle_c$ across structural subgroups for (c) faces and (d) words, with the words task showing less variance in $\langle\Delta\text{msFC}\rangle_c$ across subjects as compared to the faces task.
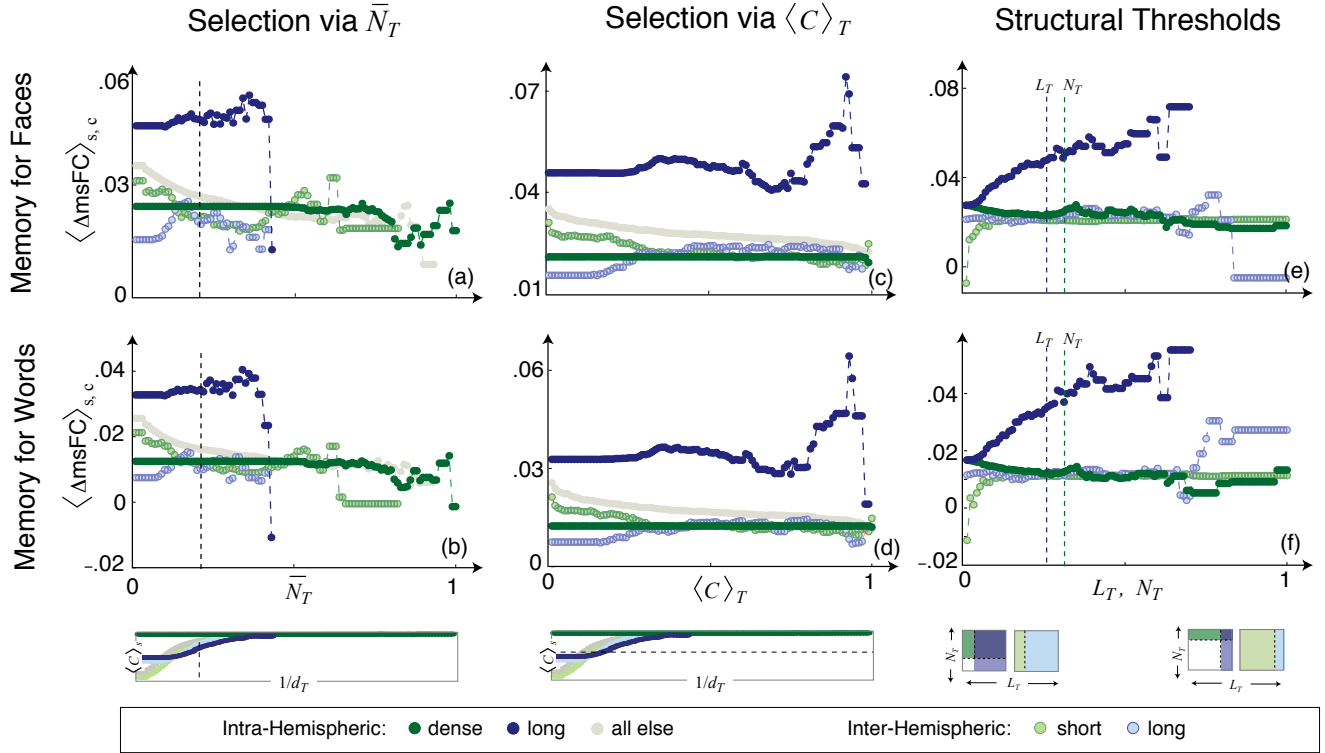
Figure S7: **Comparison of Robustness to Thresholding Between Memory for Words versus Faces.** The memory state functional connectivity $\langle \Delta\mathrm{msFC}\rangle_{\mathrm{s,c}}$ of the representative brain network shows similar robustness to region selection via $\bar{N}_T$ (left column), region selection via $\langle C\rangle_T$ (middle columns) and the structural partitions N_T and L_T (right column) between memory for faces (top row) versus memory for words (bottom row), where the trends for the faces tasks are described in detail in Figure S3 above. Across all partitions, long intra-hemispheric connections consistently show strong $\langle \Delta\mathrm{msFC}\rangle_{\mathrm{s,c}}$ for both words and faces, while inter- and dense intra-hemispheric connections show similar values of $\langle \Delta\mathrm{msFC}\rangle_{\mathrm{s,c}}$ to one another and to the remaining bulk of short, sparse intra-hemispheric connections. Interestingly, in biasing toward long connections, long inter-hemispheric connections decrease in $\langle \Delta\mathrm{msFC}\rangle_{\mathrm{s,c}}$ in the faces task but increase in $\langle \Delta\mathrm{msFC}\rangle_{\mathrm{s,c}}$ in the memory task, suggesting that these connections may be important for distinguishing between different types of memory tasks.

Furthermore, we find that memory for words shows less variation in $\langle\Delta\mathrm{msFC}\rangle_\mathrm{s}$ across connections in the representative brain network than does memory for faces (Figure S6a,b). Individual subjects show similar variation in the functional connectivity of structural subgroups between memory for words versus faces, with memory for words showing less variation in $\langle\Delta\mathrm{msFC}\rangle_\mathrm{c}$ across subjects than memory for faces (Figure S6c,d).

In a manner identical to that described in the previous section (Robustness to Thresholding), we compare the functional connectivity of memory for words versus memory for faces across variations in the selection and partitioning of region pairs in the representative brain network. Across variations in the selection thresholds $\bar{N}_T$ and $\langle C\rangle_T$, we find that memory for words shows similar qualitative shifts in $\langle\Delta\mathrm{msFC}\rangle_\mathrm{s,c}$ to those exhibited by memory for faces (see previous section for detailed discussion of threshold variations). Across variations in both selection thresholds, long intra-hemispheric connections consistently support large changes in $\langle\Delta\mathrm{msFC}\rangle_\mathrm{s,c}$ in both memory tasks (left and middle columns of Figure S7). These relationships are similarly maintained across variations in the structural thresholds N_T and L_T (right column of Figure S7). However, in biasing toward long connections, we find that very long inter-hemispheric connections show a decrease in $\langle\Delta\mathrm{msFC}\rangle_\mathrm{s,c}$ in the memory task for faces but an increase in $\langle\Delta\mathrm{msFC}\rangle_\mathrm{s,c}$ in the memory task for words. This suggests that both long inter- and long intra-hemispheric connections are important for supporting strong memory function, and long inter-hemispheric connections may be particularly important for distinguishing between different memory tasks.

Together, these results confirm that the memory state, whether defined by a memory task for words or faces, exhibits structure-function relationships that are distinct from those observed in the resting and attention states. Furthermore, these results suggest that long connections both support and distinguish between different types of memory tasks.

Inconsistent Connectivity in the Representative Brain Network

The two representative brain networks used for the separate assessments of SC $\rightarrow$ FC and FC $\rightarrow$ SC were constructed using two different, but largely overlapping, subsets of region pairs. As discussed previously (see 'Results; Overview'), regions were selected via the structural and nonstructural measures $\bar{N}$ and $1/d$. Both measures relate to but are distinct from the consistency in connectivity $\langle C\rangle_s$, where our terminology is defined such that "high consistency" and "inconsistency" in connectivity respectively refer to large and small values of $\langle C\rangle_s$. As a result of employing two different selection methods, the two representative networks vary in the degree to which regions are consistently structurally connected across subjects, as measured by the distributions of $\langle C\rangle_s$ across connections within the representative brain networks.

Identifying Inconsistent Connectivity

In the previous section (see 'Robustness to Thresholding'), we compared relationships between SC and FC across variations in the methods used to select region pairs, separately considering region pair selection via indirect ($\bar{N}$ and $1/d$, as used in the main text) versus direct ($\langle C\rangle_s$) measures of consistency. Figure S3 confirmed that the functional properties of structural subgroups are robust to the variations in consistency that arise from selecting region pairs indirectly via $\bar{N}_T$ versus directly via $\langle C\rangle_T$. Figure S4 further confirmed that the observed relationship between large connection numbers and strong rsFC is robust to similar variations in consistency arising from region pair selection via $1/d_T$ versus $\langle C\rangle_T$. However, Figure S4 showed that the apparent length of these connections varies significantly depending on region pair selection via $1/d_T$ versus $\langle C\rangle_T$. Given that $1/d$ and $\langle C\rangle_s$ are related, the question arises as to why the region pairs selected via each measure show qualitatively different relationships between $\langle L\rangle_s$ and $\langle\mathrm{rsFC}\rangle_s$.

To address this question, we note that the process of averaging structural properties across subjects can produce connections that disobey physical constraints. One such physical constraint requires that the subject-averaged length $\langle L\rangle_s$ of connections linking two regions not be less than the physical separation d between those regions. A low value of consistency $\langle C_{ij}\rangle_s$ between two regions i and j, for which a large number of subjects show no structural connectivity ($C_{ij} = 0$), can therefore be manifested in an apparent connection length $\langle L_{ij}\rangle_s$ less than the minimum physical length $L_{ij,\min} = d_{ij} - d_{\min}$, where the subtraction of the minimum interregional distance $d_{\min}$ allows for the possibility of adjacent regions to be linked via connections with near-zero length. We refer to connections that exhibit $\langle L\rangle_s < L_{\min}$ as "unphysical" connections.

We find that, within the sets of region pairs used to construct each representative brain network, a subset of region pairs exhibits this unphysical property arising from inconsistent connectivity (low values of $\langle C\rangle_s$). Figure S8a-b shows the average length $\langle L\rangle_s$ versus the inverse interregional distance $1/d$ of connections within the two representative brain networks whose region pairs were separately selected via $\bar{N}_T$ and $1/d_T$. By comparing the lengths $\langle L\rangle_s$ to the minimum physical length $L_{\min}$ (black line in Figure S8a-b), it can be seen that a fraction of connections within each network have unphysical lengths $\langle L\rangle_s < L_{\min}$. Furthermore, by comparing the distributions of $\langle C\rangle_s$ produced by connections whose lengths are greater and less than $L_{\min}$ (Figure S8c-d), we can see that this
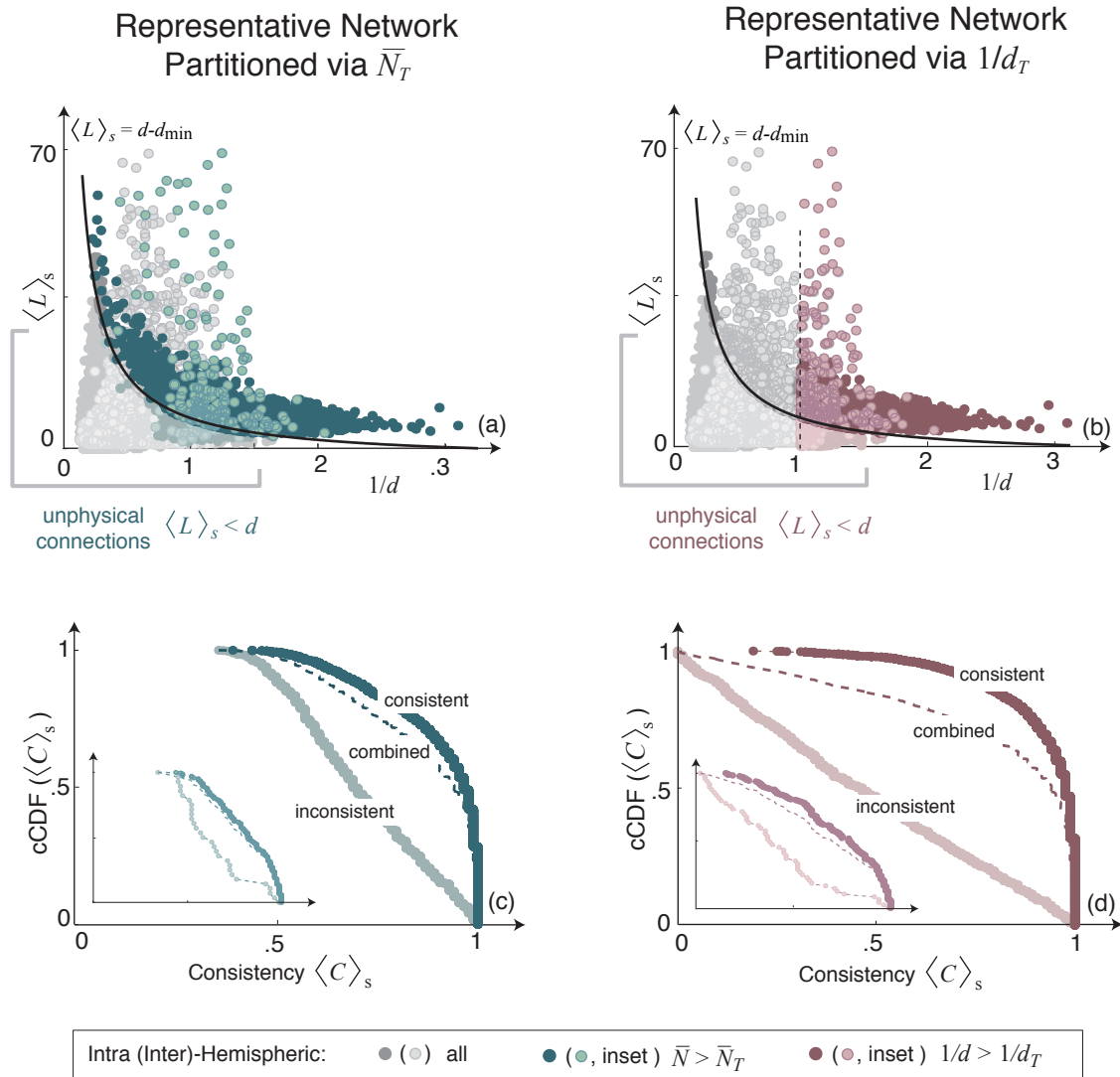
Figure S8: Inconsistent Connectivity in Representative Brain Networks. (a,c) Average length $\langle L \rangle_s$ versus inverse interregional distance $1/d$ of connections between regions within the two representative brain networks assessed in the main text. Regions selected via (a) $\bar{N}$ and (c) $1/d$ are shown respectively in turquoise and maroon, with the minimum length $L_{\min} = d - d_{\min}$ superimposed in black. Both methods of region pair selection reduce the number of, but do not eliminate, connections with unphysical lengths $\langle L \rangle_s < L_{\min}$ (opaque). The presence of unphysical connections is an artifact of averaging over connections that are inconsistently present across subjects, as evidenced in the shifted distributions of $\langle C \rangle_s$ produced by these connections (b,d). The removal of these connections shifts the average consistency toward higher values.

Consequences of Unphysical Lengths on the Inference of Function from Structure
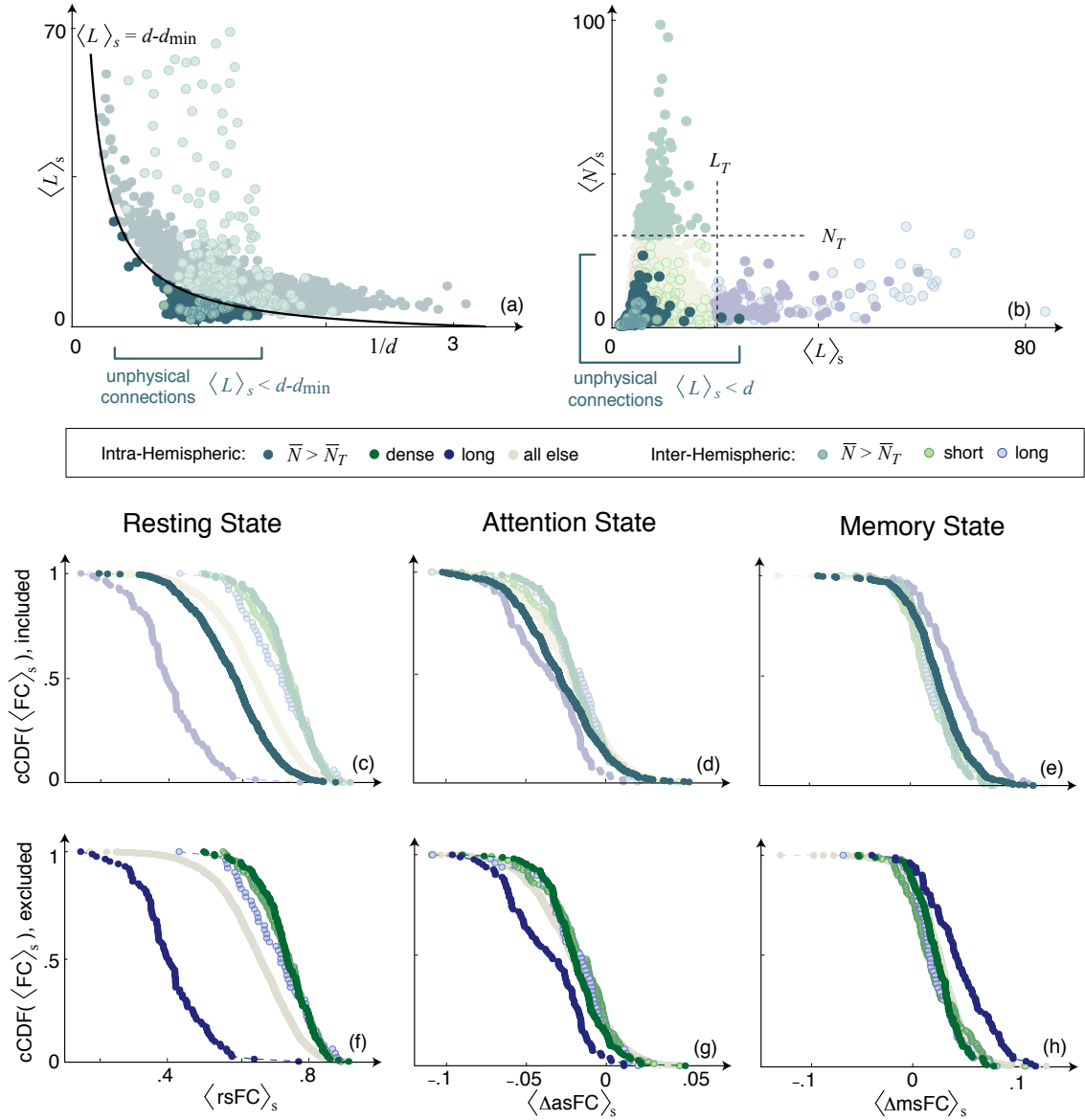
Figure S9: **Consequences of Inconsistent Connectivity on the Functional Connectivity of Structural Subgroups.** (a) The presence of unphysical average connection lengths $\langle L \rangle_s < L_{min}$ arises from inconsistently connected region pairs selected via $\bar{N}$. (b) Connections with unphysical lengths are predominantly low in number and short in length. (c-h) Distributions of average functional measures (c,f) $\langle rsFC \rangle_s$, (d,g) $\langle \Delta asFC \rangle_s$ and (e,h) $\langle \Delta msFC \rangle_s$ produced by structural subgroups of connections in the (c-e) presence and (f-h) absence of unphysical connections. As these unphysical connections predominantly fall into the large group of short, sparse intra-hemispheric connections, their presence does not qualitatively affect the observed shifts in the functional connectivity produced by inter-hemispheric, dense intra-hemispheric, and long intra-hemispheric connections.
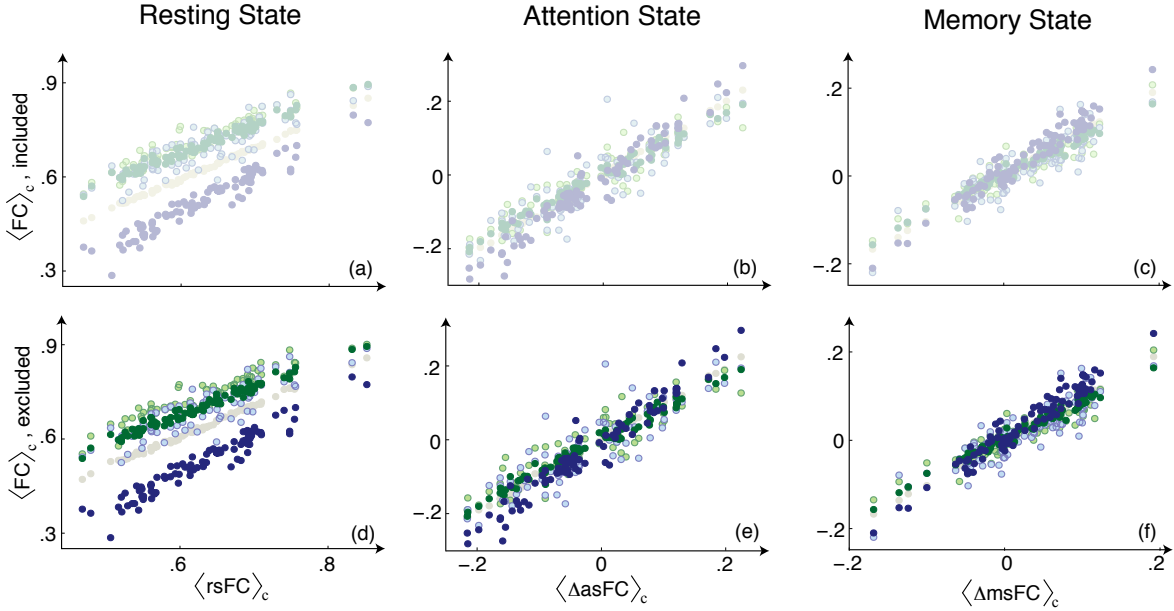
Figure S10: **Consequences of Absent Connectivity on Individual Variability in Functional Connectivity.** Absent connections (with $L = N = 0$) do not affect the average resting-state ($\langle\text{rsFC}\rangle_c$), attention-state ($\langle\Delta\text{asFC}\rangle_c$), or memory-state ($\langle\Delta\text{msFC}\rangle_c$) functional connectivity across subjects. The inclusion (top row) versus exclusion (bottom row) of absent connections produces qualitatively similar shifts in FC across subjects.

effect arises from inconsistency in connectivity. In both representative brain networks, connections with unphysical lengths less that $L_{\min}$ show significantly lower inter-subject consistency than do connections with physical lengths greater than $L_{\min}$. Because $\bar{N}$ is more strongly related to $\langle C\rangle_s$ than is $1/d$, the region pairs selected via $\bar{N}_T$ show less separation in the distributions of $\langle C\rangle_s$ than do region pairs selected via $1/d_T$.

Impact of Inconsistent Connectivity on Relationships between SC and FC

To assess the consequences of including these unphysical connection lengths within the representative brain networks, we repeat the analyses of SC $\to$ FC and FC $\to$ SC performed in the main text, now selecting regions subject to the constraints $\bar{N} > \bar{N}_T$ and $\langle L\rangle_s > L_{\min}$ (for the analysis of SC $\to$ FC) and $1/d > 1/d_T$ and $\langle L\rangle_s > L_{\min}$ (for the analysis of FC $\to$ SC).

The comparisons between this selection method and the selection via $\bar{N}_T$ and $1/d_T$ alone (as was used in the main text) are shown respectively in Figures S9 and S11. We find that, with the exception of the distribution of intra-hemispheric connection lengths inferred from rsFC (shown in Figure S9c-d and discussed below), all results remain qualitatively similar with the inclusion versus exclusion of these unphysical connections.

In the assessment of SC $\to$ FC, unphysical connections predominantly occupy the bulk of short, sparse intra-hemispheric connections (Figure S9b). Due to the large number of region pairs that fall within this structural subgroup, the relative number of region pairs linked by unphysical connection lengths is small in comparison, and therefore their inclusion does not significantly alter the observed shifts in resting-state (Figure S9c-d) or task-driven (Figure S9e-h) functional connectivity produced by different structural subgroups of connections.

In the assessment of FC $\to$ SC, unphysical connections predominantly occupy the weakly-correlated subgroup, and they show noticeably low connection numbers and lengths (Figure S11). The presence of unphysical connections increases the observed separation in connection number across functional subgroups by biasing the weakly-correlated subgroup toward lower connection numbers. The exclusion of unphysical connections from the analysis only slightly decreases, but does not remove, this separation. In comparison, the presence of unphysical connections significantly affects the distribution of connection lengths. Inspection of the length distributions shown in Figure S11d,f reveals that the inclusion of unphysical connections produces a disproportionately high density of connections with very short lengths, such that longer local connections appear to show stronger rsFC. The exclusion of unphysical connections eliminates the excess of short connection lengths, thereby altering the distributions such that increasingly strong intra-

Consequences of Unphysical Lengths on the Inference of Structure from Function
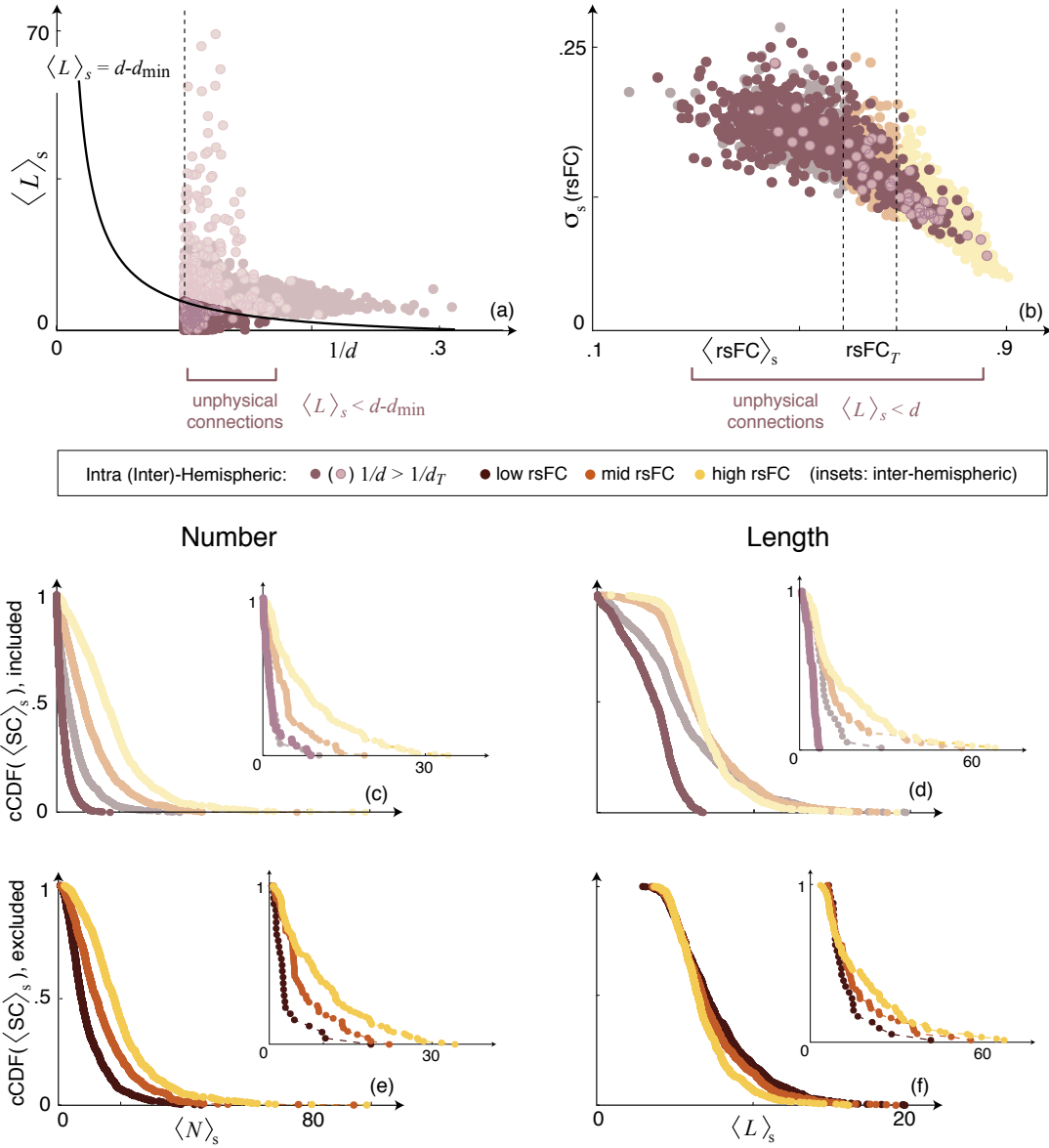

Figure S11: **Consequences of Inconsistent Connectivity on the Structural Connectivity of Functional Subgroups.** (a) Unphysical average connection lengths $\langle L \rangle_s < L_{\min}$ arising from inconsistently connected region pairs selected via $1/d$. (b) Connections with unphysical lengths predominantly link weakly-correlated intra-hemispheric regions, and therefore the removal of these connections from the analysis does not qualitatively alter the distributions of inter-hemispheric connection number or length. (c-f) Distribution of average structural measures (c,e) $\langle N \rangle_s$ and (d,f) $\langle L \rangle_s$ that support weak, intermediate, and strong correlations, shown in the (c-d) presence and (e-f) absence of unphysical connections. Inconsistent connections are (c) low in number (e) and short in length. While the presence of inconsistent connectivity does not qualitatively affect the distributions of $\langle N \rangle_s$ (d), it does significantly affect the qualitative properties of the distributions of intra-hemispheric lengths $\langle L \rangle_s$ (f). The presence of inconsistent connectivity produces a disproportionately high density of short intra-hemispheric connections, which in turn alters the relative length distributions produced by weakly- versus strongly-correlated regions. The removal of these regions from the analysis recovers a consistent relationship between increasingly short intra-hemispheric connections and increasingly strong rsFC.
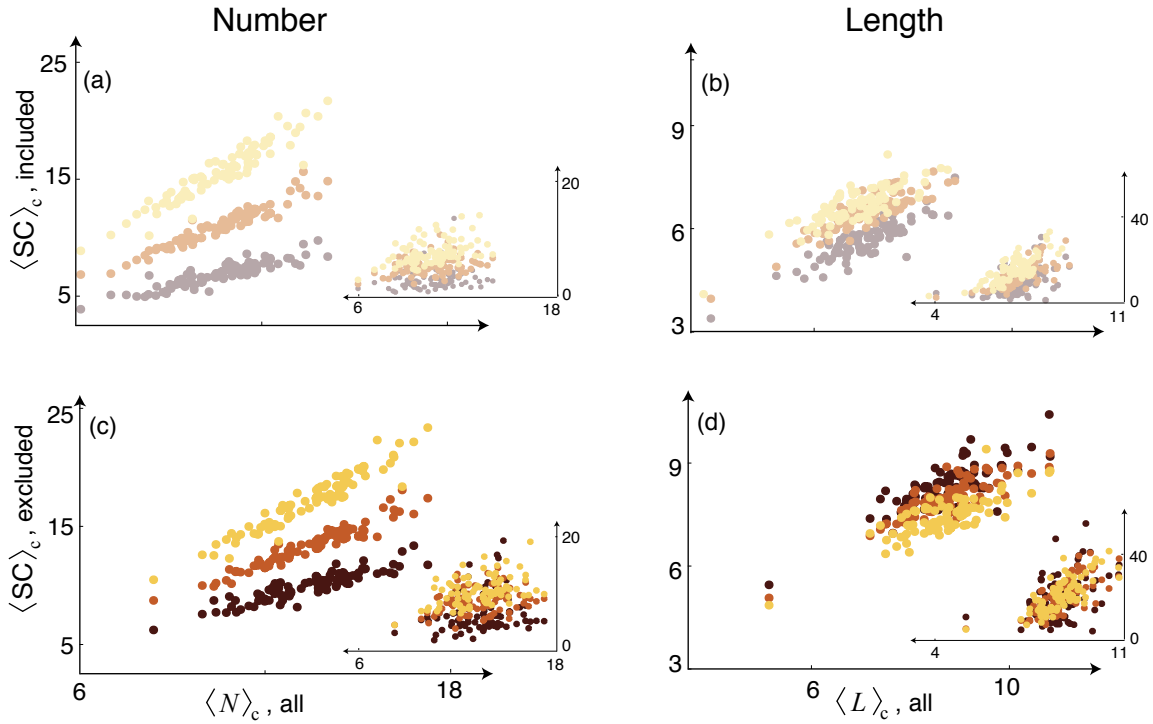
26

Figure S12: **Consequences of Absent Connectivity on Individual Variability in Structural Connectivity.** Absent connections (with $L = N = 0$) are shown to reduce, across subjects, the (a) average number $\langle N \rangle_c$ and (b) average length $\langle L \rangle_c$ of both inter- and intra-hemispheric connections. (c) Removal of absent connections from the analysis increases $\langle N \rangle_c$ across subjects while preserving the qualitative relationship between increasing $\langle N \rangle_c$ and increasing rsFC. Removal of absent connections similarly increases $\langle L \rangle_c$, but it also affects the qualitative relationship between $\langle N \rangle_c$ and rsFC. With the inclusion of absent connections, strongly-correlated intra- and inter-hemispheric regions appear to be linked by longer connections; however, the removal of absent connections shows that strongly-correlated intra-hemispheric regions are linked by shorter, rather than longer, connections, while strongly- and weakly-correlated inter-hemispheric regions show minimal differences in length. These results are consistent with those results obtained from the removal of connections with unphysical lengths in the representative brain.

hemispheric correlations are consistently supported by increasingly short connections. As was shown above (Figure S4), this finding is robust to variations in the thresholds used to both select and partition functional subgroups.

Note that a similar argument can be made to exclude connections with unphysical average numbers $\langle N \rangle_s < 1$. This constraint excludes a smaller subset of connections that is nearly fully contained within the subset excluded via $\langle L \rangle_s < L_{\min}$. This constraint therefore reduces, but does not eliminate, the altered distribution of short connection lengths. All other results remain qualitatively similar with the removal of connections with unphysical numbers.

Extension to Subject-Specific Brain Networks

Analogous techniques can be applied to single-subject networks, for which the two possible constraints imposed on representative brain networks (implemented via the exclusion of connections with $\langle L \rangle_s < L_{\min}$ or $\langle N \rangle_s < 1$) reduce to the single constraint of excluding absent connections within subject-specific networks.

Consistent with the analysis of representative brain networks, the removal of absent connections does not alter the subject-specific values of resting-state $\langle \mathrm{rsFC} \rangle_c$, attention-state $\langle \Delta \mathrm{asFC} \rangle_c$, or memory-state $\langle \Delta \mathrm{msFC} \rangle_c$ functional connectivity observed across structural subgroups (Figure S10), nor does it alter the subject-specific values of inter- and intra-hemispheric connection number $\langle N \rangle_c$ observed across functional subgroups (left column of Figure S10). However, as was observed in the representative brain network, the removal of absent connections alters the subject-specific values of inter- and intra-hemispheric connection length $\langle L \rangle_c$ (right column of Figure S10 and Figure 3f in the main text). Whereas with the inclusion of absent connections, strongly-correlated inter- and intra-hemispheric regions appear to be linked by longer connections, the removal of absent connections reveals that increasing intra-hemispheric rsFC is supported by decreasing connection lengths, while increasing inter-hemispheric rsFC shows minimal variations in connection length. These results confirm that the properties of representative brain networks are consistently observed within subject-specific networks for both the inclusion and exclusion of unphysical connections.

METHODOLOGICAL CONSIDERATIONS

In this work, we have examined functional connectivity both during rest and during the performance of attention- and memory-demanding cognitive tasks. Our work employs one possible approach for assessing brain dynamics during task performance. Alternatively, a generalized linear model (GLM) can be used in combination with techniques such as partial least squares (PLS) or psychophysiological interactions (PPI) [45, 46] to identify task-related activations across cortical and subcortical structures. Such approaches characterize brain dynamics by the level of activity, rather than the strength of connectivity, between brain regions. The relationship between activity and connectivity, however, remains poorly understood. While recent fMRI studies (e.g. [3, 47, 48]) suggest that these two measures might be correlated with one another in the resting state, the relationship between task-driven activity and connectivity is, as of yet, unknown.

Our study has several important limitations. First, we have used diffusion tensor imaging (DTI) scans, for which it is not possible to distinguish crossing fibers. The deterministic streamline tractography algorithm used here can also fail to distinguish branching fibers or fibers exhibiting abrupt turns. The use of recently-developed probabilistic tractography algorithms are expected to improve connectivity estimates in future analyses [49]. Furthermore, the tractography algorithms currently available are biased towards short fibers, and therefore the frequency of long fibers is likely underestimated in our data. We have employed an atlas-based parcellation of cortical and subcortical brain regions, which differs from surface-based parcellations in that it does not fully respect subject-specific anatomy. Therefore, the same region examined within two different subjects might contain different cortical areas, an effect that could drive some of the observed inter-subject differences in the consistency of structural connectivity.

Our fMRI preprocessing procedure has additional implications. The 600 cortical and subcortical regions constructed from the AAL atlas, while predominantly consisting of gray matter, may have contained some voxels of CSF or white matter. Signal variance in these two tissue compartments is related to physiological noise (such as heart rate and respiration) and may have contributed to the magnitude of correlation between different regions. However, the regions in the AAL atlas are defined based on gray matter tissue, and the fraction of white matter and CSF is relatively small. Furthermore, any such contribution to the inter-regional correlations would likely be constant across resting and task states. While all functional images were realigned to correct for head movements, only task-related datasets were further corrected using the robust weighted least squares analysis. As a result, it is possible that there is higher noise-driven variance in our estimates of resting-state FC as compared to attention- and memory-state FC. However, as we find no systematic pattern in head motion parameters, all of which are extremely small, we anticipate that this variance has minimal effect on our estimates of resting-state versus task-driven FC. Additional preprocessing techniques, such as global signal regression (GSR), can be used to further remove non-neuronal global signal contributions. Recent evidence suggests that the removal of such artificial coherencies may reduce variability in FC

measurements across subjects [50], and the results reported here may therefore show higher inter-subject variability in FC than could be achieved with methods such as GSR. However, as these methods can alter estimations of FC, care must be taken when interpreting the resulting analyses [51, 52].

Lastly, both structural and functional connectivity can be estimated using a variety of different measures of association. Our construction of the structural connectome employed both the number and length of white matter tracts as connection weights. Other potential choices include the average FA between regions or the curvature of tracts between regions [18]. Furthermore, alternative imaging techniques yield estimates of tract myelination [53] that can additionally be used to inform connection weights [54]. Our construction of the functional connectome employed Pearson's correlations, which are sensitive to linear relationships between time series. Alternative choices of functional connectivity measures, including nonlinear measures such as the mutual information or phase synchronization between two regional time series, may have different sensitivities to narrow and broad-band frequency information [55].

REFERENCES

[1] E. Aminoff, D. Clewett, S. Freeman, A. Frithsen, C. Tipper, A. Johnson, S. Grafton, and M. Miller, "Individual differences in shifting decision criterion: A recognition memory study," *Mem. Cogn.*, pp. 1–15, 2012.

[2] D. T. Jones, P. Vemuri, M. C. Murphy, J. L. Gunter, M. L. Senjem, M. M. M. MM, S. A. Przybelski, B. E. G. BE, K. Kantarci, D. S. K. DS, B. F. Boeve, R. C. Petersen, and C. R. J. Jr., "Non-stationarity in the "resting brain's" modular architecture," *PLoS ONE*, vol. 7, no. 6, p. e39731, 2012.

[3] D. S. Bassett, B. G. Nelson, B. A. Mueller, J. Camchong, and K. O. Lim, "Altered resting state complexity in schizophrenia," *NeuroImage*, vol. 59, no. 3, pp. 2196–2207, 2012.

[4] D. A. Fair, B. L. Schlaggar, A. L. Cohen, F. M. Miezin, N. U. Dosenbach, K. K. Wenger, M. D. Fox, A. Z. Snyder, M. E. Raichle, and S. E. Petersen, "Oxygen advection and diffusion in a three dimensional vascular anatomical network," *NeuroImage*, vol. 35, no. 1, pp. 396–405, 2007.

[5] M. E. Lynall, D. S. Bassett, R. Kerwin, P. McKenna, U. Muller, and E. T. Bullmore, "Functional connectivity and brain networks in schizophrenia," *J Neurosci*, pp. 9477–9487, 2010.

[6] D. S. Bassett, N. F. Wymbs, M. A. Porter, P. J. Mucha, J. M. Carlson, and S. T. Grafton, "Dynamic reconfiguration of human brain networks during learning," *Proc Natl Acad Sci U S A*, vol. 108, no. 18, pp. 7641–7646, 2011.

[7] M. I. Posner, "Orienting of attention," *Quarterly Journal of Experimental Psychology*, vol. 32, pp. 3–25, 1980.

[8] D. Brainard, "The psychophysics toolbox," *Spatial Vision*, vol. 10, pp. 433–436, 1997.

[9] D. G. Pelli, "The videotoolbox software for visual psychophysics: Transforming numbers into movies," *Spatial Vision*, vol. 10, pp. 437–442, 1997.

[10] D. G. Pelli, "On the relation between summation and facilitation," *Vision Research*, vol. 27, pp. 119–123, 1987.

[11] A. Watson and D. G. Pelli, "QUEST: A Bayesian adaptive psychometric method," *QUEST*, vol. 33, pp. 1–3, 1983.

[12] T. T. Liu and L. R. Frank, "Efficiency, power, and entropy in event-related fMRI with multiple trial types: Part I: theory," *NeuroImage*, vol. 21, pp. 387–400, 2004.

[13] B. Tzourio-Mazoyer, D. Landeau, F. Papathanassiou, O. Crivello, N. Etard, B. Delcroix, and M. Joliot, "Automated anatomical labeling of activations in SPM using a macroscopic anatomical parcellation of the MNI MRI single-subject brain," *NeuroImage*, vol. 15, pp. 273–289, 2002.

[14] D. B. Percival and A. T. Walden, *Wavelet Methods for Time Series Analysis*. Cambridge University Press, 2000.

[15] D. S. Bassett, A. Meyer-Lindenberg, D. R. Weinberger, R. Coppola, and E. Bullmore, "Cognitive fitness of cost-efficient brain functional networks," *Proc Natl Acad Sci USA*, vol. 106, no. 28, pp. 11747–11752, 2009.

[16] D. S. Bassett, A. Meyer-Lindenberg, S. Achard, T. Duke, and E. Bullmore, "Adaptive reconfiguration of fractal small-world human brain functional networks," *Proc Natl Acad Sci USA*, vol. 103, pp. 19518–19523, 2006.

[17] L. Deuker, E. T. Bullmore, M. Smith, S. Christensen, P. J. Nathan, B. Rockstroh, and D. S. Bassett, "Reproducibility of graph metrics of human brain functional networks," *NeuroImage*, vol. 47, no. 4, pp. 1460–1468, 2009.

[18] D. S. Bassett, J. A. Brown, V. Deshpande, J. M. Carlson, and S. T. Grafton, "Conserved and variable architecture of human white matter connectivity," *NeuroImage*, vol. 54, no. 2, pp. 1262–1279, 2011.

[19] R. Wang, T. Benner, A. G. Sorensen, and V. J. Wedeen, "Diffusion Toolkit: A software package for diffusion imaging data processing and tractography," *Proc Intl Soc Mag Reson Med*, vol. 15, no. 3720, 2007.

[20] C. Granziera, J. D. Schmahmann, N. Hadjikhani, H. Meyer, R. Meuli, V. Wedeen, and G. Krueger, "Diffusion spectrum imaging shows the structural basis of functional cerebellar circuits in the human cerebellum in vivo," *PLoS One*, vol. 4, no. 4, p. e5101, 2009.

[21] V. J. Wedeen, R. P. Wang, J. D. Schmahmann, T. Benner, W. Y. Tseng, G. Dai, D. N. Pandya, P. Hagmann, H. D'Arceuil, and A. J. de Crespigny, "Diffusion spectrum magnetic resonance imaging (DSI) tractography of crossing fibers," *NeuroImage*, vol. 41, no. 4, pp. 1267–1277, 2008.

[22] M. Wahl, Z. Strominger, R. J. Jeremy, A. J. Barkovich, M. Wakahiro, E. H. Sherr, and P. Mukherjee, "Variability of homotopic and heterotopic callosal connectivity in partial agenesis of the corpus callosum: a 3T diffusion tensor imaging and Q-ball tractography study," *AJNR Am J Neuroradiol*, vol. 30, no. 2, pp. 282–289, 2009.

[23] M. S. Vishwas, T. Chitnis, R. Pienaar, B. C. Healy, and P. E. Grant, "Tract-based analysis of callosal, projection, and association pathways in pediatric patients with multiple sclerosis: a preliminary study," *AJNR Am J Neuroradiol*, vol. 31, no. 1, pp. 121–128, 2010.

[24] M. Lagana, M. Rovaris, A. Ceccarelli, C. Venturelli, S. Marini, and G. Baselli, "DTI parameter optimisation for acquisition at 1.5T: SNR analysis and clinical application," *Comput Intell Neurosci*, p. 254032, 2010.

[25] M. Nezamzadeh, V. J. Wedeen, R. Wang, Y. Zhang, W. Zhan, K. Young, D. J. Meyerhoff, M. W. Weiner, and N. Schuff, "In-vivo investigation of the human cingulum bundle using the optimization of MR diffusion spectrum imaging," *Eur J Radiol*, vol. 75, no. 1, p. e29, 2010.

[26] S. Mori, B. J. Crain, V. P. Chacko, and P. C. van Zijl, "Three-dimensional tracking of axonal projections in the brain by magnetic resonance imaging," *Ann Neurol*, vol. 45, no. 2, pp. 265–269, 1999.

[27] S. Mori and P. C. van Zijl, "Fiber tracking: principles and strategies - A technical review," *NMR Biomed*, vol. 15, pp. 468–480, 2002.

[28] R. Xue, P. C. van Zijl, B. J. Crain, M. Solaiyappan, and S. Mori, "In vivo three-dimensional reconstruction of rat brain axonal projections by diffusion tensor imaging," *Magn Reson Med*, vol. 42, pp. 1123–1127, 1999.

[29] G. Gong, Y. He, L. Concha, C. Lebel, D. W. Gross, A. C. Evans, and C. Beaulieu, "Mapping anatomical connectivity patterns of human cerebral cortex using in vivo diffusion tensor imaging tractography," *Cereb Cortex*, vol. 19, no. 3, pp. 524–536, 2009.

[30] N. Shu, Y. Liu, J. Li, Y. Li, C. Yu, and T. Jiang, "Altered anatomical network in early blindness revealed by diffusion tensor tractography," *PLoS One*, vol. 4, no. 9, p. e7228, 2009.

[31] R. S. Desikan, F. Segonne, B. Fischl, B. T. Quinn, B. C. Dickerson, D. Blacker, R. L. Buckner, A. M. Dale, R. P. Maguire, B. T. Hyman, M. S. Albert, and R. J. Killiany, "An automated labeling system for subdividing the human cerebral cortex on MRI scans into gyral based regions of interest," *NeuroImage*, vol. 31, no. 3, pp. 968–980, 2006.

[32] P. Hagmann, L. Cammoun, X. Gigandet, R. Meuli, C. J. Honey, V. J. Wedeen, and O. Sporns, "Mapping the structural core of human cerebral cortex," *PLoS Biol*, vol. 6, no. 7, p. e159, 2008.

[33] A. Fornito, A. Zalesky, D. Bassett, D. Meunier, M. Yücel, S. J. Wood, D. Nertney, B. Mowry, C. Pantelis, and E. Bullmore, "Genetic influences on cost-efficient organization of human cortical functional networks," *J Neurosci*, vol. 31, no. 9, pp. 3261–3270, 2010.

[34] H. J. H. andG. R. Mangun, W. Burchert, H. Hinrichs, M. Scholz, T. F. Munte, A. Gos, M. Scherg, S. Johannes, H. Hundeschagen, M. S. Gazzaniga, and S. A. Hillyard, "Combined spatial and temporal imaging of brain activity during visual selective attention in humans," *Nature*, vol. 372, pp. 543–546, 1994.

[35] S. Fu, P. M. Greenwood, and R. Parasurama, "Brain mechanisms of involuntary visuospatial attention: An event-related potential study," *Hum. Brain Mapp.*, vol. 25, pp. 378–390, 2005.

[36] S. L. Fairhall, I. Indovina, J. Driver, and E. Macaluso, "The brain network underlying serial visual search: Comparing overt and covert spatial orienting, for activations and for effective connectivity," *Cereb. Cortex*, vol. 19, no. 12, pp. 2946–2958, 2009.

[37] H. Burianova and C. L. Grady, "Common and unique activations in autobiographical, episodic, and semantic retrieval," *J. Cog. Neurosci.*, vol. 19, pp. 1520–1534, 2007.

[38] A. Martin and L. L. Chao, "Semantic memory and the brain: structure and processes," *Curr. Opin. Neurobiol.*, vol. 11, pp. 194–201, 2001.

[39] H. Burianova, A. R. McIntosh, and C. L. Grad, "A common functional brain network for autobiographical, episodic, and semantic memory retrieval," *NeuroImage*, vol. 49, pp. 865–874, 2010.

[40] R. S. Rosenbaum, M. Ziegler, G. Winocur, C. L. Grady, and M. Moscovitch, "I have often walked down this street before: fMRI studies on the hippocampus and other structures during mental navigation of an old environment," *Hippocampus*, vol. 14, pp. 826–835, 2004.

[41] D. A. Gusnard, E. Akbudak, G. L. Shulman, and M. E. Raichle, "Medial prefrontal cortex and self-referential mental activity: relation to a default mode of brain function," *Proc. Natl. Acad. Sci. U. S. A.*, vol. 98, pp. 4259–4264, 2001.

[42] M. Kaiser and C. C. Hilgetag, "Modeling the development of cortical systems networks," *Neurocomputing*, vol. 58, pp. 297–302, 2004.

[43] R. Salvador, J. Suckling, M. R. Coleman, J. D. Pickard, D. Menon, and E. Bullmore, "Neurophysiological architecture of functional magnetic resonance images of human brain," *Cereb Cortex*, vol. 15, pp. 1332–1342, 2005.

[44] C. J. Honey, O. Sporns, L. Cammoun, X. Gigandet, J. P. Thiran, R. Meuli, and P. Hagmann, "Predicting human resting-state functional connectivity from structural connectivity," *Proc Natl Acad Sci U S A*, vol. 106, no. 6, pp. 2035–2040, 2009.

[45] A. Krishnan, L. J. Williams, A. R. McIntosh, and H. Abdi, "Partial least squares (pls) methods for neuroimaging: a tutorial and review.," *NeuroImage*, vol. 56, no. 2, pp. 455–475, 2011.

[46] J. X. O'Reilly, M. W. Woolrich, T. E. Behrens, S. M. Smith, and H. Johansen-Berg, "Tools of the trade: psychophysiological interactions and functional connectivity," *Soc. Cogn. Affect. Neurosci.*, vol. 7, no. 5, pp. 604–609, 2012.

[47] A. Zalesky, A. Fornito, G. F. Egan, C. Pantelis, and E. T. Bullmore, "The relationship between regional and inter-regional functional connectivity deficits in schizophrenia," *Hum. Brain Mapp.*, vol. 33, no. 11, pp. 2535–2549, 2012.

[48] N. Petridou, C. C. Gaudes, I. L. Dryden, S. T. Francis, and P. A. Gowland, "Periods of rest in fmri contain individual spontaneous events which are related to slowly fluctuating spontaneous activity," *Hum. Brain Mapp.*, 2012.

[49] G. J. Parker and D. C. Alexander, "Probabilistic Monte Carlo based mapping of cerebral connections utilising whole-brain crossing fibre information," *Information Processing in Medical Imaging*, vol. 18, pp. 684–695, 2003.

[50] H. He and T. T. Liu, "A geometric view of global signal confounds in resting-state functional MRI," *NeuroImage*, vol. 59, pp. 2339–2348, 2011.

[51] K. Murphy, R. M. Birn, D. A. Handwerker, T. B. Jones, and P. A. Bandettini, "The impact of global signal regression on resting state correlations: are anti-correlated networks introduced?," *NeuroImage*, vol. 44, no. 3, pp. 893–905, 2009.

[52] A. Weissenbacher, C. Kasess, F. Gerstl, R. Lanzenberger, E. Moser, and C. Windischberger, "Correlations and anticorrelations in resting-state functional connectivity MRI: a quantitative comparison of preprocessing strategies," *NeuroImage*, vol. 47, no. 4, pp. 1408–1416, 2009.

[53] M. P. van den Heuvel, R. C. Mandl, C. J. Stam, R. S. Kahn, and H. E. Hulshoff Pol, "Aberrant frontal and temporal complex network structure in schizophrenia: a graph theoretical analysis," *J Neurosci*, vol. 30, no. 47, pp. 15915–15926, 2010.

[54] M. Rubinov and D. S. Bassett, "Emerging evidence of connectomic abnormalities in schizophrenia," *J Neurosci*, vol. 31, no. 17, pp. 6263–6265, 2011.

[55] O. David, D. Cosmelli, and K. J. Friston, "Evaluation of different measures of functional connectivity using a neural mass model," *NeuroImage*, vol. 21, pp. 659–673, 2004.